The effects of UV background correlations on Lyα forest flux statistics

Avery Meiksin[1], Martin White[2]
[1] *Institute for Astronomy, University of Edinburgh, Blackford Hill, Edinburgh EH9 3HJ, UK*
[2] *Departments of Astronomy and Physics, University of California, Berkeley, CA 94720, USA*

12 November 2018

ABSTRACT
We examine the possible effects of UV background fluctuations on the pixel flux power spectrum and auto-correlation function of the Lyα forest due to a finite number of sources in an attenuating medium. We consider scenarios in which QSO sources dominate the contribution to the UV background. To estimate their contribution, we use the QSO luminosity functions from the 2dF and the Sloan Digital Sky Survey. We estimate self-consistent values for the attenuation length at the Lyman edge through the Intergalactic Medium using Particle Mesh simulations of the Lyα forest, normalised by the measured mean Lyα flux. It is necessary to add the contribution from Lyman Limit Systems based on their measured statistical properties since the simulations are unable to reproduce the measured abundances of these systems, suggesting their formation may involve more complex hydrodynamical processes than simple collapse into dark matter halos. We examine the convergence properties of the flux power spectrum and auto-correlation function under differing assumptions regarding pressure-smoothing. Convergence to better than 10% in the flux power spectrum at proper wavenumbers $k < 0.015\,(\mathrm{km\,s^{-1}})^{-1}$ requires a comoving resolution of $30-60\,h^{-1}\,\mathrm{kpc}$ in a comoving box of size $25\,h^{-1}\,\mathrm{Mpc}$ at $z=5$, with the requirements becoming more severe at lower redshifts. The flux auto-correlation function does not converge to better than 10% on scales exceeding 3% of the box size. We find much better covergence properties for the *relative* effects of the UV background fluctuations on the flux power spectrum. The background fluctuations increase the large-scale power and suppress the power at intermediate scales. At $z \leq 4$, the effect is only at the few percent level. By $z > 5$, however, the large-scale power is boosted by more than 50%, suggesting the flux power spectrum may serve as a useful tool for distinguishing QSO-dominated UV background scenarios from those in which more abundant sources like galaxies dominate.

Key words: methods: numerical – intergalactic medium – quasars: absorption lines

1 INTRODUCTION

Due in large part to insights gained from hydrodynamical simulations of structure formation in the universe (Cen et al. 1994; Zhang, Anninos & Norman 1995; Hernquist et al. 1996; Zhang et al. 1997; Bond & Wadsley 1997; Theuns, Leonard & Efstathiou 1998) the Lyα forest, as measured in high redshift Quasi-Stellar Object (QSO) spectra, has emerged as one of our premier probes of the universe at high redshift. The results of simulations assuming early homogeneous H I and He II reionization reproduce the cumulative flux distributions and H I column density distributions measured from high resolution spectra to an accuracy of a few percent (Meiksin, Bryan & Machacek 2001). More problematic are the predicted widths of the absorption features, which appear to require additional sources of broadening, perhaps late He II reionization, to match the measured widths (Theuns et al. 1999; Bryan & Machacek 2000; Meiksin et al. 2001).

Parallel to the development of the full hydrodynamical simulations of the Intergalactic Medium (IGM) are pseudo-hydrodynamical schemes using pure gravity (Petitjean, Mücket & Kates 1995; Croft et al. 1998; Gnedin & Hui 1998; Meiksin & White 2001). These simpler treatments are based on two key results from the full hydrodynamical computations. As a consequence of photoionization equilibrium: 1. the gas follows a tight temperature–density relation for the absorbing material with the neutral hydrogen temperature proportional to the baryon density to the power of ~ 0.5 (Zhang et al. 1998; Schaye et al. 1999), and 2. the neutral hydrogen density closely traces the total matter density on the scales relevant to the forest ($0.1 - 10\,h^{-1}$Mpc) (Zhang

et al. 1998). The structure in QSO absorption thus tracks, in a calculable way, slight fluctuations in the matter density of the universe back along the line of sight to the QSO, with most of the absorption by the Lyα forest arising from gas with overdensities of a few times the mean density. Although these techniques are not sufficiently accurate to be used for detailed modelling of the flux and absorption line properties of the IGM (Meiksin & White 2001), they provide a useful means of investigating convergence questions and the possible role of additional physical effects on the Lyα forest without the substantial overhead of the full hydrodynamical treatment. In particular, in recent years they have been increasingly relied on for predicting the flux power spectrum of the Lyα forest (Meiksin & White 2001; Zaldarriaga, Hui & Tegmark 2001; Croft et al. 2002b; Seljak, McDonald & Makarov 2003).

While much work has been done on the physics of the Lyα forest and the cosmology which may be extracted, the role of fluctuations in the UV background on the absorption properties of the Lyα forest are largely unexplored (see Zuo 1992a,b; Fardal & Shull 1993; Croft et al. 1999, 2002a; Gnedin & Hamilton 2002). The effects of fluctuations in the UV background on the statistical properties of the Lyα forest were considered previously by Zuo (1992a,b) and Zuo & Phinney (1993). Zuo & Bond (1994) introduced the use of the flux transmission auto-correlation function for measuring the clustering of the absorbing gas, although they did not consider the effect of fluctuations in the UV background apart from a local proximity effect. As we shall show, the effects of UV background correlations are most conspicuous only at high redshifts ($z > 5$), where the precise level of absorption by the Lyα forest is most difficult to measure because of the extremely low flux values, requiring very high signal-to-noise ratio spectra.

Fardal & Shull (1993) explored the effects of UV background fluctuations on the Lyα forest along the lines of Zuo, but using Monte Carlo realisations of randomly distributed sources and clouds to estimate the effect of the background fluctuations. Croft et al. (1999) estimated the flux power spectrum resulting from UV background fluctuations generated by randomly distributed QSO sources in a uniform IGM, and found this to be small, at the few percent level, compared with the flux power spectrum from the Lyα forest at $z = 2.5$. They found that allowing for QSO clustering had little additional effect. Croft et al. (2002a) accounted for the UV background fluctuations at $z = 3$ assuming the IGM was ionized by the galaxies in their simulation, and concluded again the effect on the flux power spectrum is small. Finally Gnedin & Hamilton (2002) examined the effect of a fluctuating UV background at $z = 4$ using hydro simulations with pseudo-radiative transfer, assuming the reionization is accomplished by galaxies in their simulation. They concluded the fluctuations of the UV background affect the flux power spectrum at the percent level, but cause an underestimate of the photo-ionization rate by $\mathcal{O}(20\%)$. A comparable boost in the photo-ionization rate is required if QSOs are the dominant source of the UV background at $z \geq 5$ (Paper I).

In this paper, we investigate the effect of the fluctuations on the 2-pt flux distribution (the power spectrum and auto-correlation function) of the Lyα forest. This extends our earlier work on the 1-pt distribution function reported in Meiksin & White (2003; hereafter Paper I). In the next section we describe the simulations used. In Section 3, we discuss our model for the UV background fluctuations. The results are presented in Section 4, and we summarise our conclusions in Section 5. In Appendix A we discuss the numerical convergence tests we've performed, and we describe our estimates of the mean Lyα flux in Appendix B.

Model	Ω_M	Ω_v	$\Omega_b h^2$	h	n	σ_8	σ_J
1	0.30	0.70	0.020	0.70	1.05	0.97	1.59
2	0.35	0.65	0.020	0.70	0.95	0.88	1.35
3	0.40	0.60	0.020	0.55	1.10	0.90	1.57
4	0.30	0.70	0.022	0.70	0.95	0.92	1.32
C	0.30	0.70	0.018	0.67	1.00	0.90	1.28

Table 1. Parameters for the cosmological models. Ω_M is the total mass density parameter, Ω_v the vacuum energy density parameter, Ω_b the baryonic mass fraction, $h = H_0/100\,\mathrm{km\,s^{-1}\,Mpc^{-1}}$, where H_0 is the Hubble constant at $z = 0$, n the slope of the primordial density perturbation power spectrum, σ_8 the fluctuation normalization at $z = 0$ in a sphere of radius $8h^{-1}$ Mpc, and σ_J the fluctuation normalization at $z = 3$ filtered on the Jeans scale for gas at $T = 2 \times 10^4$ K.

2 NUMERICAL SIMULATIONS

To investigate the effects of UV background fluctuations on the power spectrum of the Lyα forest, we have performed simulations of 5 different cosmological models within the ΛCDM family. In each case we used pure Particle Mesh (PM) dark matter simulations, mimicking the temperature of the gas using a polytropic equation of state and assuming gas and dark matter have the same spatial distribution. This has been shown (Petitjean, Mücket & Kates 1995; Croft et al. 1998; Gnedin & Hui 1998; Meiksin & White 2001), to produce results comparable to the full hydrodynamical simulations at the level of 10 per cent. The agreement is expected to be even better on the large scales of interest to this work. The parameters for the simulations are provided in Table 1. The models are all for a flat universe and are consistent with Lyα forest constraints on matter fluctuations σ_J on the Jeans scale (Meiksin, Bryan & Machacek 2001). Models 1–3 were run previously to the WMAP results and were constructed to be consistent with existing large-scale structure, cluster abundance, and CMB constraints at the time. Model 4 was later added explicitly to be consistent with WMAP results as well (Verde et al. 2003, Hinshaw et al. 2003, Kogut et al. 2003). Although Models 1–3 are not the best matches to the recent WMAP data, they are close to models that are good matches on the scales relevant to the Lyα forest. We provide in Table 2 a list of similar models with their χ^2 agreement to the WMAP TT data. Model C is the concordance model of Ostriker & Steinhart (1995). A description of the parallel PM code used is given in Paper I. In each case we used 512^3 particles and a 1024^3 force mesh, in a cubic box with (comoving) side length $25\,h^{-1}$Mpc, except for Model C, for which the comoving box size was $30\,h^{-1}$Mpc.

Ω_M	Ω_v	$\Omega_b h^2$	h	n	τ	σ_8	σ_J	χ^2
0.30	0.70	0.020	0.70	0.95	0.10	0.912	1.31	1020.5
0.30	0.70	0.020	0.70	0.95	0.15	0.958	1.38	1030.7
0.30	0.70	0.020	0.70	1.00	0.10	0.954	1.46	1040.8
0.30	0.70	0.020	0.70	1.00	0.15	1.000	1.54	1041.0
0.30	0.70	0.022	0.70	0.95	0.15	0.920	1.32	990.1
0.30	0.70	0.022	0.70	1.00	0.10	0.917	1.40	992.7
0.30	0.70	0.022	0.70	1.00	0.15	0.961	1.46	990.7
0.30	0.70	0.024	0.70	1.00	0.10	0.881	1.33	984.0
0.30	0.70	0.024	0.70	1.00	0.15	0.921	1.39	979.7
0.30	0.70	0.020	0.75	0.95	0.10	1.068	1.59	1212.1
0.35	0.65	0.020	0.65	0.95	0.10	0.901	1.32	1001.2
0.35	0.65	0.020	0.65	0.95	0.15	0.942	1.38	1008.2
0.35	0.65	0.020	0.65	1.00	0.10	0.940	1.47	1042.3
0.35	0.65	0.020	0.65	1.00	0.15	0.982	1.54	1039.1
0.35	0.65	0.022	0.65	0.95	0.15	0.907	1.32	986.2
0.35	0.65	0.022	0.65	1.00	0.10	0.903	1.40	1013.8
0.35	0.65	0.022	0.65	1.00	0.15	0.946	1.47	1008.1
0.35	0.65	0.024	0.65	1.00	0.10	0.866	1.34	1025.5
0.35	0.65	0.024	0.65	1.00	0.15	0.907	1.40	1017.6
0.35	0.65	0.024	0.70	0.95	0.10	0.987	1.49	1022.0

Table 2. Parameters for cosmological models consistent with WMAP data. Ω_M is the total mass density parameter, Ω_v the vacuum energy density parameter, Ω_b the baryonic mass fraction, $h = H_0/100\,\mathrm{km\,s^{-1}\,Mpc^{-1}}$, where H_0 is the Hubble constant at $z = 0$, n the slope of the primordial density perturbation power spectrum, τ is the Thomson optical depth to the last scattering surface, σ_8 the fluctuation normalization at $z = 0$ in a sphere of radius $8h^{-1}$ Mpc, σ_J the fluctuation normalization at $z = 3$ filtered on the Jeans scale for gas at $T = 2 \times 10^4$ K, and the values of χ^2 are from fits to the WMAP TT data.

z	$\langle\exp(-\tau)\rangle$	Γ_{-12}	r_0	N_0	$N_{\rm box}$
6.0	< 0.006	< 0.14	< 23.0	3.9	1.2
5.5	$0.079^{+0.017}_{-0.013}$	$0.37^{+0.06}_{-0.05}$	77^{+13}_{-9}	130	1.0
5.0	$0.12^{+0.03}_{-0.04}$	$0.31^{+0.07}_{-0.09}$	85^{+17}_{-22}	200	1.2
4.0	0.36 ± 0.03	$0.43^{+0.06}_{-0.05}$	80 ± 5	240	1.7
4.0	0.47 ± 0.03	$0.76^{+0.12}_{-0.11}$	104 ± 6	510	1.7
3.89	0.48 ± 0.02	$0.68^{+0.08}_{-0.07}$	106 ± 5	560	1.8
3.0	0.70 ± 0.02	$0.88^{+0.14}_{-0.12}$	211 ± 11	5900	2.4
2.75	0.74 ± 0.04	$0.86^{+0.36}_{-0.24}$	250 ± 28	1.1×10^4	2.6

Table 3. Some of the output times for the simulations. For each redshift the mean Lyα flux, $\langle\exp(-\tau)\rangle$, the required H I photoionization rate, in units of $10^{-12}\,\mathrm{s^{-1}}$, to recover the mean flux assuming a homogeneous UV background, the attenuation length r_0, in comoving h^{-1}Mpc, and the mean number of sources per attenuation volume, N_0, are listed for Model 4. The last column, $N_{\rm box}$, shows the number of sources in the simulation volume of side $25\,h^{-1}$Mpc (comoving). The two values at $z = 4.0$ correspond to two disparate estimates of the mean Lyα flux.

Convergence tests, described in Appendix A, suggest that these scales are adequate for our purposes.

Given a set of final particle positions and velocities, we compute the spectra as follows. First the density and density-weighted line-of-sight velocity are computed on a grid (using CIC interpolation) and smoothed using FFT techniques. We try three different smoothing schemes, as described below and in Appendix A. The default scheme simply smooths with a Gaussian of width one grid cell. This forms the fundamental data set. A regular grid of 32×32 sightlines is drawn through the box, parallel to the box sides. Along each sightline we integrate (in real space) to find $\tau(u)$ at a given velocity u. Specifically we define

$$\tau(u) = \int dx\, A(x) \left[\frac{\rho(x)}{\bar\rho}\right]^2 T(x)^{-0.7} b^{-1} e^{-(u-u_0)^2/b^2} \qquad (1)$$

where $u_0 = xaHL_{\rm box} + v_{\rm los}$ and $b = \sqrt{2k_BT/m_{\rm H}}$ is the Doppler parameter, where $m_{\rm H}$ is the mass of a hydrogen atom. The flux at velocity u is $\exp(-\tau)$. The integration variable x indicates the distance along the box in terms of the expansion velocity across the box. In evaluating Eq. (1) we assume a power-law relation between the gas density and temperature

$$T \equiv T_0 \left(\frac{\rho}{\bar\rho}\right)^{\gamma-1} \qquad (2)$$

In practice, T_0 and γ will depend on the reionization history of the IGM, but we shall fix $T_0 = 2 \times 10^4$K and $\gamma = 1.5$ throughout as described in Paper I.

In terms of the baryon density parameter Ω_b, hydrogen baryonic mass fraction X, the metagalactic photoionization rate Γ_{-12}, in units of $10^{-12}\,\mathrm{s^{-1}}$, and the number f_e of electrons per hydrogen nucleus, the function $A(x)$ is given by:

$$A(x) = 18.0 f_e \left(\frac{X}{0.76}\right)\left(\frac{\Omega_b h^2}{0.02}\right)\Gamma_{-12}^{-1}(x) L_{\rm box}(1+z)^5, \qquad (3)$$

where $\Gamma_{-12}(x)$ is evaluated at position x, $L_{\rm box}$ is in Mpc and b in eq. (1) is in $\mathrm{km\,s^{-1}}$. We normalise the spectra according to measurements of the mean absorbed flux $\langle\exp(-\tau)\rangle$ as reported in Fan et al. (2002) (their Figure 1) for $z \geq 4$. We discuss the values adopted at other redshifts in Appendix B. Values for $\langle\exp(-\tau)\rangle$ at each of the output times of the simulation are provided in Table 3.

In order to compute the flux power spectra, it is necessary to filter the simulation data to reduce the effects of particle noise at the grid level. The minimal amount of filtering we consider is Gaussian smoothing on the scale of a mesh cell. While this is appropriate for computing the power spectrum of the dark matter, it neglects any 'natural' filtering arising from pressure forces acting on the baryons. The most accurate means of predicting the power spectrum is by performing full hydrodynamical simulations at both high spatial resolution and in a box of sufficient size to ensure convergence. Such calculations, however, are still prohibitively expensive to repeat for a range of models, and also because the origin of the line broadening is not fully understood (Theuns et al. 1999; Bryan & Machacek 2000;

Meiksin et al. 2001), requiring additional modelling which affects both the shape and amplitude of the predicted flux power spectrum. As we are primarily interested in the *relative* effect of fluctuations in the UV background, we do not consider an exhaustive range of smoothing procedures, but only consider a few straightforward ones to judge how important smoothing is to our final results. Following Gnedin & Hui (1998), in addition to the minimal smoothing models, we create models with additional smoothing on scales of the order of the Jeans length. Specifically we compute a 'Jeans scale', $k_J = (3/2)^{1/2} c_s^{-1} H(z)/(1+z)$, where c_s is the sound speed, using the assumed temperature and equation of state of the gas and used this in place of our one mesh cell filtering above. We consider two different types of smoothing, a Gaussian of width $\sigma = 2^{1/2} k_J$ and a form motivated by linear perturbation theory, viz. $(1 + [k/k_J]^2)^{-1}$. We emphasize again that all of these approaches, like the pseudo-hydrodynamical approach employed by McDonald (2003), are ad hoc and can only be justified by comparison to true hydrodynamic simulations, but modify the power mostly on scales where thermal broadening is also very important.

3 UV BACKGROUND

3.1 UV intergalactic attenuation

For the uniform background case, normalising the simulation results by the mean Lyα flux also fixes the attenuation properties of the IGM since the ionization structure of the IGM has been fixed by the normalisation. This was exploited in Paper I to place constraints on the attenuation length r_0 and mean emissivity required to recover the measured values of the mean Lyα flux for $z > 4$. At lower redshifts, the simulation results are no longer sufficient for determining the Lyman limit optical depth of the IGM. We find that the simulations fail to reproduce the measured number of Lyman Limit Systems (LLSs) by a factor of several. A similar conclusion was reached by Gardner et al. (1997) on the basis of lower resolution simulations than those we present. There, the authors attempted to correct for the missing LLSs by estimating the contribution from unresolved halos on the basis of Press-Schechter theory. They found that they still fell well short of the observed number. Our simulations resolve halos down to masses of about $10^8 - 10^9\, M_\odot$, corresponding to circular velocities smaller than $20 - 25\,\mathrm{km\,s^{-1}}$ at $z = 3$. The baryons in smaller mass halos would be heated to temperatures too high to remain bound after photoionization (Meiksin 1994), so that smaller mass halos would seem unlikely candidates for LLSs. We again find too few LLSs. This suggests that the origin of these systems may involve more complex hydrodynamical processes than simple collapse into dark-matter halos, such as Jeans fragmentation in the halos (Meiksin 1994), tidal streaming or galactic winds.

In order to estimate the attenuation length, we adopt the measured abundance of LLSs from Stengler-Larrea et al. (1995) for $\tau_L > 1$, $dN/dz = N_0(1+z)^\gamma$, with $N_0 = 0.25^{-0.10}_{+0.17}$ and $\gamma = 1.50 \pm 0.39$ for $0.3 \lesssim z \lesssim 4$. The contribution of the LLSs to the effective optical depth of the IGM at the Lyman edge is given by (Zuo 1992b)

$$\tau_{\rm eff}^L = \int_{z_{\rm obs}}^{z_{\rm em}} dz \int_1^\infty d\tau_L \frac{\partial^2 N}{\partial z \partial \tau_L} \left\{ 1 - \exp\left[-\tau_L \left(\frac{1+z_{\rm obs}}{1+z} \right)^3 \right] \right\}. \quad (4)$$

Here, the optical depth corresponds to the path between the source at $z_{\rm em}$ and the position of observation at $z_{\rm obs}$. Because of the difficulty in measuring the high optical depths involved, the actual distribution of individual Lyman limit optical depths is less certain. Adopting a power law distribution $\partial^2/\partial z \partial \tau_L = A(1+z)^\gamma \tau_L^{-\beta}$, and assuming a flat universe so that $dz/dr_p \approx (H_0 \Omega_M^{1/2}/c)(1+z)^{5/2}$ where r_p is proper length, we obtain

$$\frac{d\tau_{\rm eff}^L}{dr_p} \approx \frac{H_0 \Omega_M^{1/2}}{c} N_0 (1+z)^{5/2+\gamma} \left[1 - e^{-1} + \Gamma(2-\beta, 1) \right], \quad (5)$$

where $\Gamma(a,x)$ is the incomplete $\Gamma-$function. Adopting $\Omega_M = 0.3$, $h = 0.7$, $N_0 = 0.25$, $\gamma = 1.50$, we obtain $d\tau_{\rm eff}^L/dr_p \approx 3.2 \times 10^{-5} \mathcal{T} (1+z)^4$, where $\mathcal{T} = 0.85$ for $\beta = 2$ and 0.91 for $\beta = 1.5$. In the limit of an infinitely steep distribution, so that all systems have $\tau_L = 1$, $\mathcal{T} = 0.63$.

To estimate the total Lyman limit optical depth through the IGM, we add the LLS contribution to the values we find from a given simulation for $z \leq 4$. Current measurements do not permit an estimate of the LLS contribution at higher redshifts. Given the uncertain origin of these systems, we conservatively do not include them in our estimates for $z > 4$. Doing so would result in a decrease of the attenuation length. We also assume the proper source emissivity does not evolve in our estimate of the attenuation length. Over the range of measured optical depths, this assumption only weakly affects our results.

In Fig.1, we show the redshift evolution of $d\tau_{\rm eff}^L/dr_p$ from the simulation results for Model 4, along with the range in the LLS contribution based on observations. We also show the evolution of the attenuation length, defined by $r_0 = (d\tau_{\rm eff}^L/dr_p)^{-1}$, and compare our estimate with previous estimates based on direct Lyα forest line counts from Meiksin & Madau (1993) and Haardt & Madau (1996). We have included the LLS contribution to the attenuation lengths for $z \leq 4$. We also show the effect including the LLS contribution, if extrapolated to $z \geq 5$, would have on r_0 by the open points at $z = 5$ and 5.5. Our estimates for the attenuation length lie between the medium and low attenuation models of Meiksin & Madau (1993), and lie systematically above the estimate of Haardt & Madau (1996). The redshift dependence of the (proper) attenuation lengths we find is fit by $r_0 \approx 6800\, h^{-1}\,\mathrm{Mpc}\,(1+z)^{-3.5}$ over $2.75 \leq z \leq 5.5$ to $\sim 20\%$ accuracy. The attenuation lengths allowing for an extrapolation of the LLS contribution to $z > 4$ are fit over the same redshift range by $r_0 \approx 1.7 \times 10^4\, h^{-1}\,\mathrm{Mpc}\,(1+z)^{-4.2}$ to $\sim 10\%$ accuracy. We caution against extending the fits outside the specified redshift range. In particular, we find the attenuation length decreases precipitously between $z = 5.5$ and 6, a consequence of the observed sharp rise in the Lyα optical depth at these redshifts (Fan et al. 2002).

3.2 Source contribution

The QSO luminosity function has a slope at the bright end varying as $\phi(L) \propto L^{-\beta_1}$, where $\beta_1 = 3.41$ according to the 2dF QSO sample for $z < 2.3$ (Boyle et al. 2000), and $\beta_1 = 2.58$ according to the Sloan QSO sample for $z > 3.5$ (Fan et al. 2001), although $\beta_1 = 3.2$ is still permitted by the data.

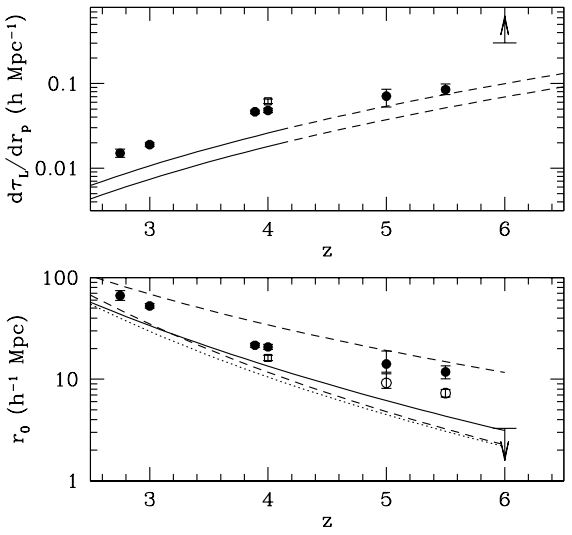

Figure 1. The (proper) gradient $d\tau_L/dr_p$ of the Lyman limit optical depth (upper panel) and the (proper) attenuation length (lower panel) for Model 4. The points are estimated from the simulation results using the observational constraints on the mean Lyα flux. The contribution from Lyman Limit Systems is included in the values of the attenuation length for $z \leq 4$. The effect Lyman Limit Systems would have on the attenuation length at $z = 5$ and 5.5 is shown by the open points. The open square at $z = 4$ corresponds to an alternative lower estimate for the average absorbed flux (see text). The two solid curves in the upper panel show the upper and lower limits for the measured contribution from Lyman Limit Systems, with the dashed extensions extrapolations based on the lower redshift measurements. The two dashed lines in the lower panel are based on the low and high attenuation models of Meiksin & Madau (1993), and the solid line is based on their medium attenuation model. The dotted line is based on the attenuation estimate of Haardt & Madau (1996).

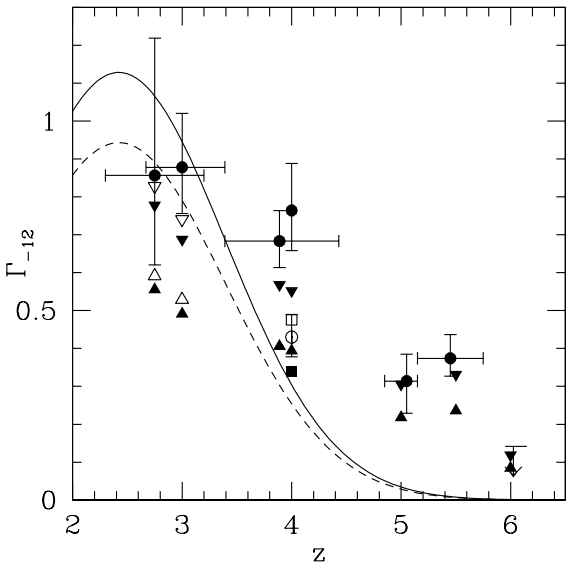

Figure 2. A comparison between the estimated H I metagalactic photoionization rate Γ_{-12} from QSO sources and the rate required to match the measured mean Lyα flux, as estimated for Model 4. The filled data points with error bars are from Table 3. The open data point at $z = 4$ is for an alternative lower estimate of the mean Lyα flux (see text). The estimated rates for QSO sources, shown by the filled triangles, assume a QSO luminosity function with a steep end slope of $\beta_1 = 3.2$. The inverted filled triangles include a 40% boost, nearly the maximum possible contribution from diffuse recombination radiation emitted by the IGM. The open triangles and inverted triangles are analogous estimates assuming $\beta_1 = 3.41$. The filled square at $z = 4$ is for $\beta_1 = 3.2$ and the alternative lower mean Lyα flux considered. The open square includes a 40% boost in this estimate due to diffuse radiation from the IGM. Also shown are the estimates from Haardt & Madau (1996) based on earlier QSO source counts and assuming an intrinsic QSO spectral index shortward of the Lyman edge of $\alpha_Q = 1.5$ (solid line) and $\alpha_Q = 1.8$ (dashed line), and which include the diffuse recombination radiation from the IGM.

We use the procedure in Paper I for adjusting the parameters of the Boyle, Shanks & Peterson (1988) luminosity function,

$$\Phi(L) = \frac{\Phi^*}{[(L/L^*)^{\beta_1} + (L/L^*)^{\beta_2}]}, \tag{6}$$

viz., by fixing $\beta_2 = 1.58$, in accordance with Boyle et al. (2000), and matching the SDSS counts for $M_{1450} < -25.7$ for $z < 6$ and for $M_{1450} < -27.1$ at $z = 6$ (and allowing for differences in the assumed values of the Hubble constant). We show the predicted contribution of QSOs to Γ_{-12} in Fig. 2 for $\beta_1 = 3.2$, and compare these with the required rates from Table 3. We have followed the procedure of Paper I for estimating Γ_{-12} from the QSO emissivity, including hardening of the metagalactic radiation field on filtering through the IGM (Haardt & Madau 1996). Specifically, for $z \leq 3$ we assume a metagalactic spectral index $\alpha_{\rm MG} = 0$, while for $3.89 \leq z \leq 5.5$ we take $\alpha_{\rm MG} = -1.3$, except at $z = 5.0$ ($\alpha_{\rm MG} = -0.5$) and $z = 6$ ($\alpha_{\rm MG} = 0$). These values were chosen to recover the required photoionization rates within 2σ, though usually the addition of some diffuse radiation is required. The value of $\alpha_{\rm MG}$ is uncertain and can only be computed fully self-consistently by solving the detailed radiative transfer problem through the high redshift IGM, but we do not expect it to deviate much from the values we use. In any case, the spectral index only weakly affects the overall ionization rate after integrating over the photoelectric cross-section. Significant diffuse radiation resulting from re-radiation by the IGM through radiative recombinations is expected at these high redshifts (Meiksin & Madau 1993; Haardt & Madau 1996), with as much as a $(\alpha_A - \alpha_B)/\alpha_A \approx 40 - 50\%$ boost in the total metagalactic photoionization rate over the direct contribution from the QSO sources. We show the enhanced rates for a 40% boost in Fig. 2.

The QSO contribution to the metagalactic photoionization rate lies systematically below the required values at $z = 3 - 4$. Given the uncertainties in the required rates, as well as in the QSO counts at these redshifts, it is unclear how seriously the discrepancy should be taken. Based on a different estimate of the QSO counts, Haardt & Madau

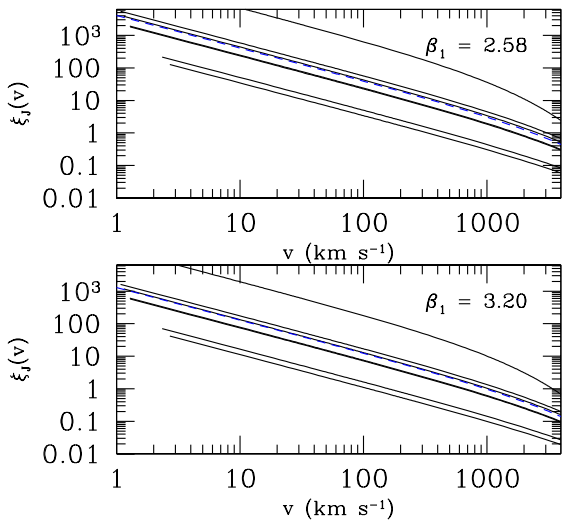

Figure 3. The auto-correlation function in the UV background predicted from QSO sources with $\beta_1 = 2.58$ (upper panel) and $\beta = 3.20$ (lower panel). The solid curves, from top to bottom, correspond to the redshifts $z = 6$, 5.5, 5, 4, 3.89, 3, and 2.75. The $z = 4$ solid curve is computed for a (comoving) attenuation length of $r_0 = 104h^{-1}$ Mpc and nearly coincides with the $z = 3.89$ result. Also shown is the result at $z = 4$ assuming $r_0 = 80h^{-1}$ Mpc (dashed line), which nearly coincides with the $z = 5$ result.

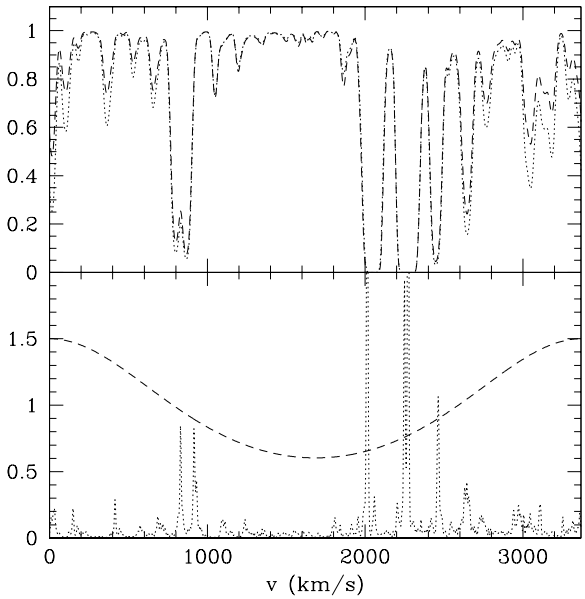

Figure 4. A simulated spectrum from a 'typical' sightline at z=5 from Model 1. The upper panel shows the spectrum with a uniform ionizing background ($A(x) \equiv$const, dashed) and where the UV background comes from a single source situated at the center of the box (dotted). The lower panel shows $0.1 \times \rho/\bar{\rho}$ (dotted) and $A(x)/\bar{A}$ (dashed) for the single source case.

(1996) compute a photoionization rate that well matches the required rate at $z \approx 3$ (see Fig. 2), although their value lies much below the required rate by $z = 4$. (A required slower rate of decline at $z \gtrsim 3$ than predicted by Haardt & Madau was also found by Meiksin, Bryan & Machacek 2001.) A boost in the IGM temperature at these redshifts, as expected for late He II reionization (Madau & Meiksin 1994; Reimers et al. 1997; Meiksin, Bryan & Machacek 2001), would also help ease the discrepancy (because of the resulting reduced hydrogen recombination rate). Finally, if the luminosity from QSO sources is beamed, the estimated UV contribution would increase like the ratio of the UV beam solid angle to the optical beam solid angle, since the QSO counts are based on restframe optical or near UV (longward of the Lyman edge) surveys. (In principle, this could also result in a decrease in the estimated QSO contribution to the UV background if the ratio were less than unity.) None the less, it is interesting in this context that Steidel, Pettini & Adelberger (2001) report a large Lyman-continuum emissivity from Lyman-break galaxies at $z \simeq 3.4$. Adjusting their value down by the factor $\Omega_M^{1/2}$ for Model 4, the predicted photoionization rate at $z = 3$, assuming a non-evolving proper emissivity, is $\Gamma_{-12} = 4.4$, well in excess of the required value in Table 3. Within the context of our models, such a high rate would so reduce the neutral fraction of the H I that the IGM would become significantly more transparent to Lyα photons than measured. To match our estimated 3σ upper limit on the photoionization rate would require the Lyman-continuum emitting phase of the Lyman-break galaxy population to last only over a redshift interval $\Delta z \approx 0.1$. Thus the required excess photoionization above the QSO contribution could be accounted for by the Lyman-break galaxies, but only if they are a bursting population at these redshifts. Based on population synthesis models of the galaxies, Ferguson, Dickinson & Papovich (2002) argue this indeed may be the case.

3.3 UV background fluctuations

We compute the auto-correlation function of the QSO contribution to the UV background, using the formalism of Zuo (1992b) (also see Paper I), both for $\beta_1 = 2.58$ and 3.2. The results are shown in Fig. 3. Formally the correlation function diverges at zero separation, since the variance in the radiation field diverges (Zuo 1992a; Paper I). The typical width of an absorption feature is $25\,\mathrm{km\,s^{-1}}$, so when the correlations become small on this scale, we expect them to have a negligible influence on the flux auto-correlations or power spectra. We find that for $z > 3$, the correlations still exceed unity on this scale, so that we may expect the effect of UV background fluctuations to imprint a signature on the flux statistics of the Lyα forest. We note that for $\beta_1 = 2.58$, additional sources (like galaxies) must be introduced to recover the required H I photoionization rate (Paper I), but that these sources would only dilute the correlations by a factor of 2–3.

The effect of a discrete source on the Lyα flux is shown in Fig. 4. Here we artificially suppose that the entire UV background flux comes from a single source located in the center of the simulation box. For a line-of-sight which passes

slightly off center the $A(x)$ and spectrum are as shown, along with the spectrum that would have resulted along this sightline if the UV background were completely uniform.

To model the fluctuations in the UV background from a 'realistic' population of discrete sources we resort to a Monte Carlo procedure. We create random source lists, with luminosities drawn from the QSO luminosity function above. A random number of QSOs is chosen consistent with the luminosity density of QSOs with absolute magnitude at rest-frame 1450A $M_{1450} < -18.5$. The luminosity of each QSO is drawn at random from the luminosity function, and the sources are distributed at random positions in a volume larger than the size of the simulation box. We choose the box size to be sufficiently large to include the full effects of attenuation but not so large that redshift or evolution effects become important, so that the box is not larger than the effective size over which sources contribute to the local UV intensity (no larger than l_U in Paper I).

The frequency specific flux at the Lyman edge is then calculated at each position on the simulation grid from

$$f_L = \sum_i L_i \frac{e^{-r_i/r_0}}{4\pi r_i^2} \tag{7}$$

where the sum is over the sources, the specific luminosity of source i at the Lyman edge is L_i, and r_i is the distance of the ith source from the fiducial point in the simulation volume. To convert from the QSO luminosity at 1450A to the Lyman edge, we adopt a QSO spectral shape of the form $f_\nu \sim \nu^{-0.99}$ from $1050 - 1450$A and $f_\nu \sim \nu^{-1.8}$ from $912 - 1050$A (Zheng et al. 1997). Since our simulation box, and the relevant attenuation lengths, is small we do not keep track of source lifetimes or lightcone effects (see Croft 2003). To compute the total rate Γ_{-12} of ionizing photons (in units of $10^{-12}\,\mathrm{s}^{-1}$), from $f_L(x)$, we adjust the spectral index of the metagalactic background to reproduce the target values of $\langle\exp(-\tau)\rangle$ in Table 3. As in the uniform UV background case, for $z \geq 3.89$ the required values are generally negative ($-1.3 \lesssim \alpha_{\rm MG} \lesssim -0.5$), consistent with the expected hardening of the radiation field near the Lyman edge on being filtered through the IGM. Other sources, like galaxies, may of course contribute as well. Adjusting $\alpha_{\rm MG}$ to reproduce the required ionization rate provides an upper limit to the possible effects of UV background correlations resulting from attenuation; the introduction of additional sources would tend to dilute these effects. We also consider cases with a diffuse radiation field, as is expected to arise from radiative recombinations within the IGM.

Once we have Γ_{-12} throughout the simulation volume, we compute $A(x)$. We ignore the fluctuations in the IGM temperature that would result, noting that this is another possible contribution to the flux power spectrum, but one again that requires detailed modelling of the reionization process. Since our simulation volume is small, we explicitly checked that imposing periodic boundary conditions on the flux distribution modified our results by much less than 1 per cent.

We run sufficient realizations of this procedure to ensure convergence (one to several hundred, depending on redshift), keeping track of the UV background and flux correlation functions and the flux power spectrum. This enables us to compute both the mean spectra and their correlations.

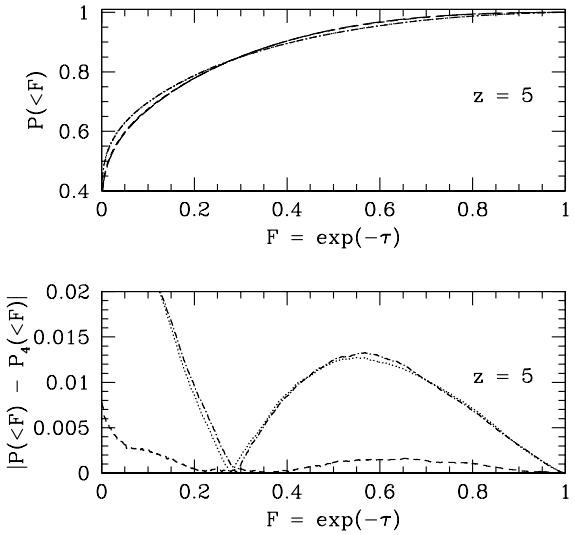

Figure 5. (Top panel) The cumulative distributions of the pixel flux at $z = 5$ for the four models assuming no UV background fluctuations. The models are labelled as Model 1 (dotted), Model 2 (short dashed), Model 3 (dot-short dashed), Model 4 (long dashed). The distributions group according to the value of σ_J, flattening as σ_J increases. (Bottom panel) The differences between the cumulative flux distributions for Models 1–3 and the distribution for Model 4 assuming no UV background fluctuations at $z = 5$. (The line types correspond to those in the top panel.)

4 RESULTS

4.1 Pixel flux distribution

The cumulative pixel flux distributions at $z = 5$ are shown in Fig. 5. The slopes of the distributions are determined essentially by the value of σ_J, and show a systematic trend of flattening with increasing σ_J. The same trend was found by Meiksin et al. (2001) at $z = 3$, who exploited it to place stringent constraints on σ_J from high spectral resolution measurements of the Lyα forest. These results corroborate the trend found there. For a single high resolution spectrum of typically $N_{\rm pix} = 10^4$ pixels, it is possible to distinguish the cumulative distributions only to differences of about $1/N_{\rm pix}^{1/2} = 0.01$, or somewhat larger allowing for pixel flux correlations (Meiksin, Bryan & Machacek 2001), so that while Models 1 and 3 could be distinguished from Model 4, Model 2 could not on the basis of a single spectrum.

The effect of fluctuations in the UV background on the cumulative flux distributions for Model 4 at $z = 4$, 5, 5.5 and 6 is shown in Fig. 6. As found in Paper I, the UV background fluctuations produce only a small distortion on the pixel flux distribution. The distortions found here are somewhat larger than found in Paper I, because here we now also account for correlations in the UV background. As found in Paper I, the effects of the UV background fluctuations are generally smaller than or comparable to the uncertainty between models with differing values of σ_J. Only at the smallest flux values (< 0.1) would it be possible to distinguish the

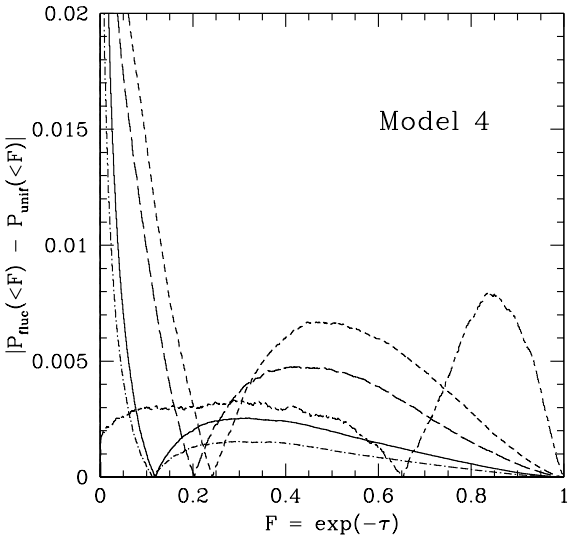

Figure 6. The differences between the cumulative flux distributions for Model 4 with and without UV background fluctuations, at $z = 4$ (short-long dashed), 5 (short dashed), 5.5 (long dashed) and 6 (solid). Also shown is the difference at $z = 6$ allowing for a diffuse component added to the fluctuating UV background (dot-short dashed).

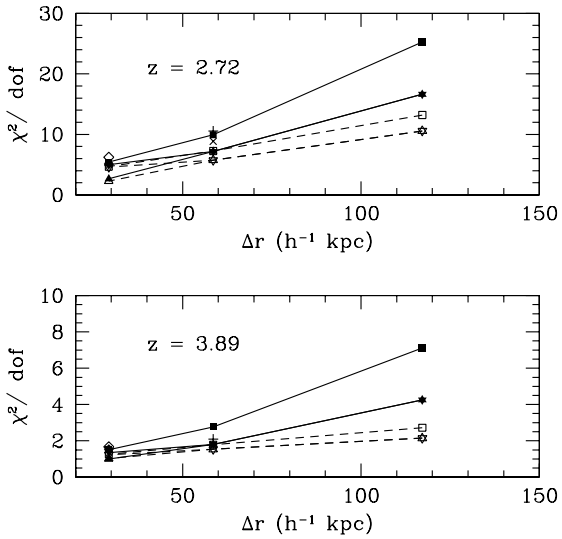

Figure 8. The χ^2 per degree of freedom between the concordance model and the measured flux power spectrum $P_F(k)$, as a function of (comoving) resolution. The upper panel is for z=2.7, and the lower for z=3.9. The open symbols use all points with $k < 0.015\,(\mathrm{km\,s^{-1}})^{-1}$, and the filled symbols use all points with $k < 0.032\,(\mathrm{km\,s^{-1}})^{-1}$. The results are shown for the $30\,\mathrm{h^{-1}}$ Mpc (comoving) box simulations, for Gaussian smoothing on the mesh scale (triangle), Gaussian Jeans smoothing (inverted triangle), and Gaussian linear smoothing (square). Also shown is the Gaussian mesh-size smoothing case for the $60\,\mathrm{h^{-1}}$ Mpc (comoving) box simulation for $k < 0.015\,(\mathrm{km\,s^{-1}})^{-1}$ (+) and $k < 0.032\,(\mathrm{km\,s^{-1}})^{-1}$ (×), as well as the results using alternative equations of state (open and filled diamonds) for the $30\,\mathrm{h^{-1}}$ Mpc high resolution box (see text). To help guide the eye, filled symbols are connected by solid lines and open symbols by dashed lines.

effects of the fluctuations from an uncertainty in the model if the model is known with sufficient accuracy. A comparable level of uncertainty is introduced by the uncertain equation of state of the gas (Paper I), but this may be removed by adjusting the temperature to match the measured distributions of Doppler parameters or wavelet coefficients (Meiksin 2000; Meiksin, Bryan & Machacek 2001).

As in Paper I, we find that the demands on the mean photoionization rate increase in the presence of UV background fluctuations. Allowing for the correlations in the UV background, however, reduces the effect, and it actually inverts by $z = 6$. Specifically, for $z \leq 5.5$ we find the mean photoionization rate must increase by 5–10% when the (correlated) UV background fluctuations are included in the models. The amount of the increase depends on the fractional contribution arising from a diffuse radiation field and on the redshift. At $z = 6$, the required mean photoionization rate is instead reduced by 10-20% when the now strongly correlated UV background fluctuations are included.

4.2 Pixel flux power spectrum

We compute the flux power spectrum at wavenumber k for the spectra according to

$$P_F(k) = \langle|\widehat{\delta f}|^2\rangle/\langle f\rangle^2, \tag{8}$$

where $\widehat{\delta f}$ denotes the Fourier transform of $\delta f = f - \langle f\rangle$. In order to assess the accuracy of our predicted flux power spectra, we compare the results for Models 1 and 4 and the concordance model with the measurements of McDonald et al. (2000) at $z = 3.89$, 3.00 and 2.41, using spectra normalised to the identical mean Lyα flux they report. The results are shown in Fig. 7. The same models are compared with the data of Croft et al. (2002b) at 2.72 (using the simulation results at $z = 2.75$). Since Croft et al. report no mean Lyα flux measurement for their spectra, we adopt the value in Table 3. We note that according to eq.(26) of Croft et al. , Model 1 is ruled out at the 3.9σ level, while Model 4 and the concordance models at only the 1.0σ and 1.9σ levels, respectively. At $z = 2.7$, we find Model 1 fits about as well as Model 4 and the concordance model. For $k < 0.015\,(\mathrm{km\,s^{-1}})^{-1}$, the χ^2 for Models 1, 4 and the concordance model, compared with the data of Croft et al. , are, respectively, 13.8, 16.5 and 18.3. The respective probabilities $P(> \chi^2)$ for the 8 $k-$values are 0.087, 0.036 and 0.019, so that Model 1 is actually preferred.

In order to understand the differences between our results and those of Croft et al. , we have performed a resolution sequence of comparisons between the concordance model simulations and the measurements, for a fixed equation of state (ie, leaving T_0 and γ unchanged). In Fig. 8 we show how the reduced χ^2 varies with resolution, for both $k < 0.015\,(\mathrm{km\,s^{-1}})^{-1}$ and $k < 0.032\,(\mathrm{km\,s^{-1}})^{-1}$. (The simu-

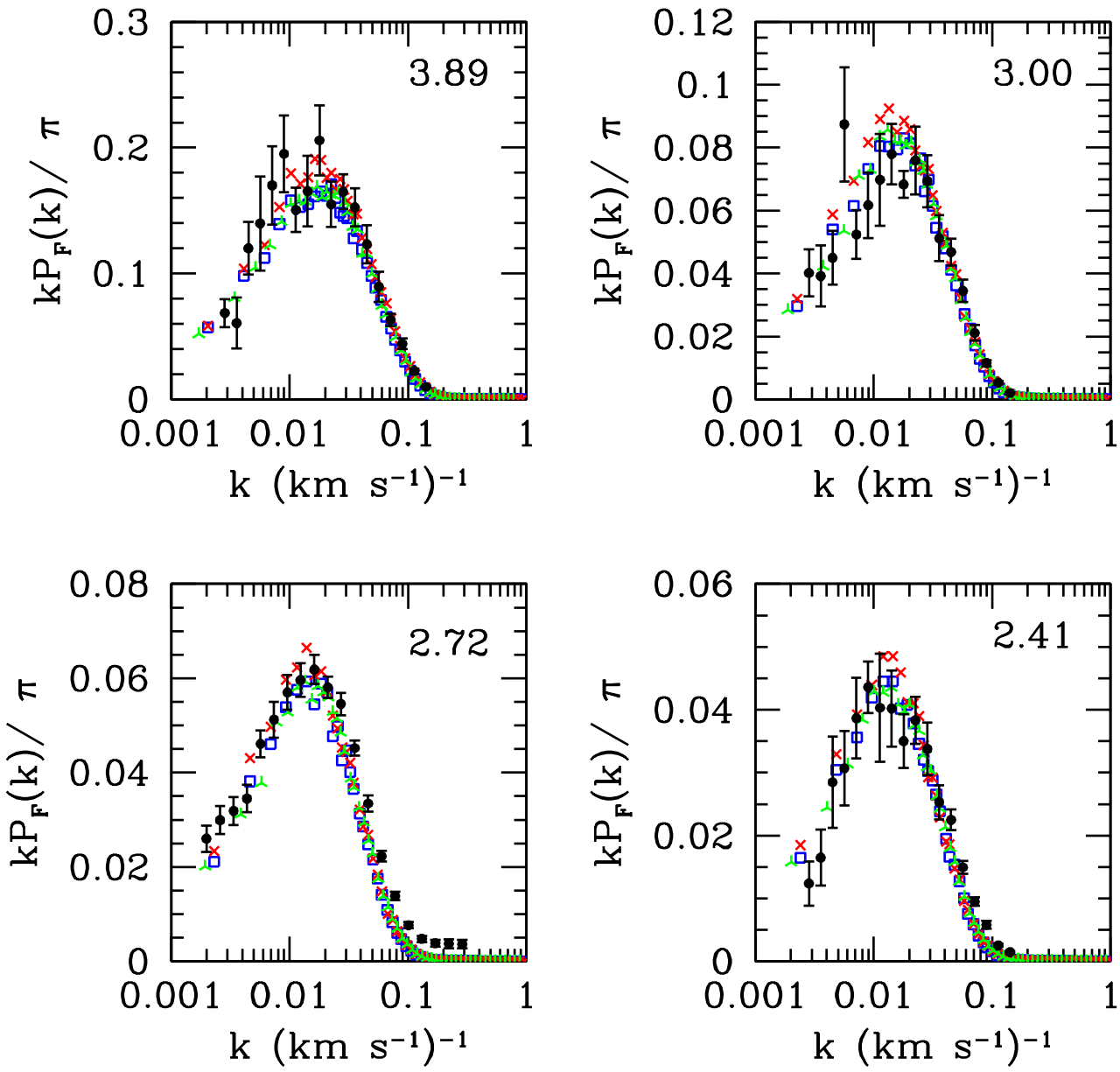

Figure 7. The flux power spectrum $P_F(k)$, as a function of restframe velocity wavenumber, for Models 1 (×) and 4 (square) and the concordance model (inverted Y), compared with the measurements in high resolution spectra at the indicated redshifts.

lation values are linearly interpolated to the $k-$values of the measured $P_F(k)$ points.) We do the comparison for mesh-scale smoothing, Gaussian Jeans smoothing and linear Jeans smoothing. A clear trend of diminishing χ^2 with increasing resolution is apparent in all cases, showing that the lower resolution simulations have not yet matched the precision of the measured $P_F(k)$ values. Only at the highest resolution do the simulations begin to converge, giving values of sufficient precision to make a meaningful comparison with the measured values. The decrease in χ^2 at higher resolution is

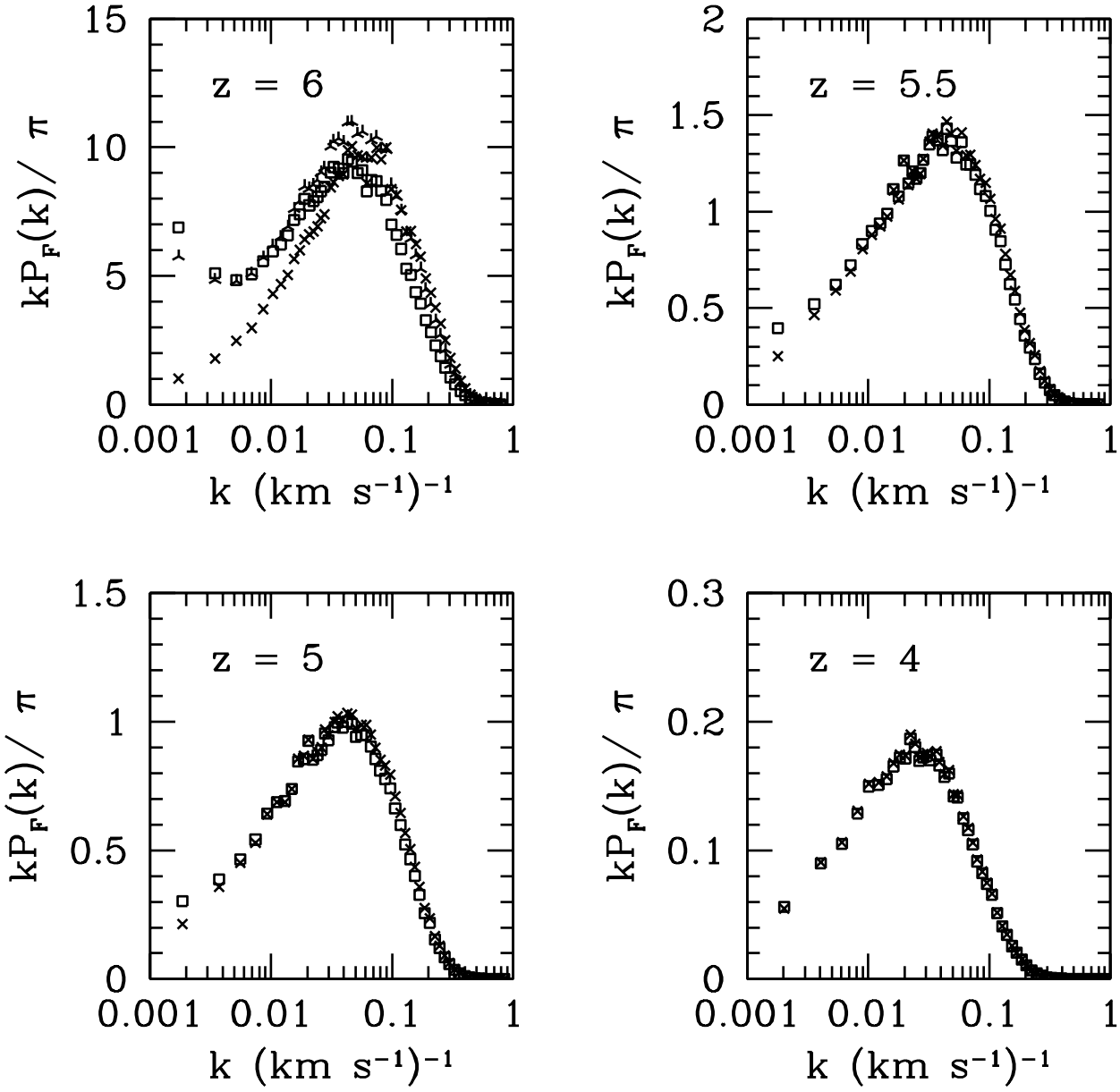

Figure 9. The flux power spectrum $P_F(k)$, as a function of restframe velocity wavenumber, for Model 4, with (square) and without (×) UV background fluctuations. Also shown is $P_F(k)$ at $z = 6$ allowing for a slight suppression due to diffuse radiation (inverted Y). The results are shown at $z = 4$, 5, 5.5 and 6.

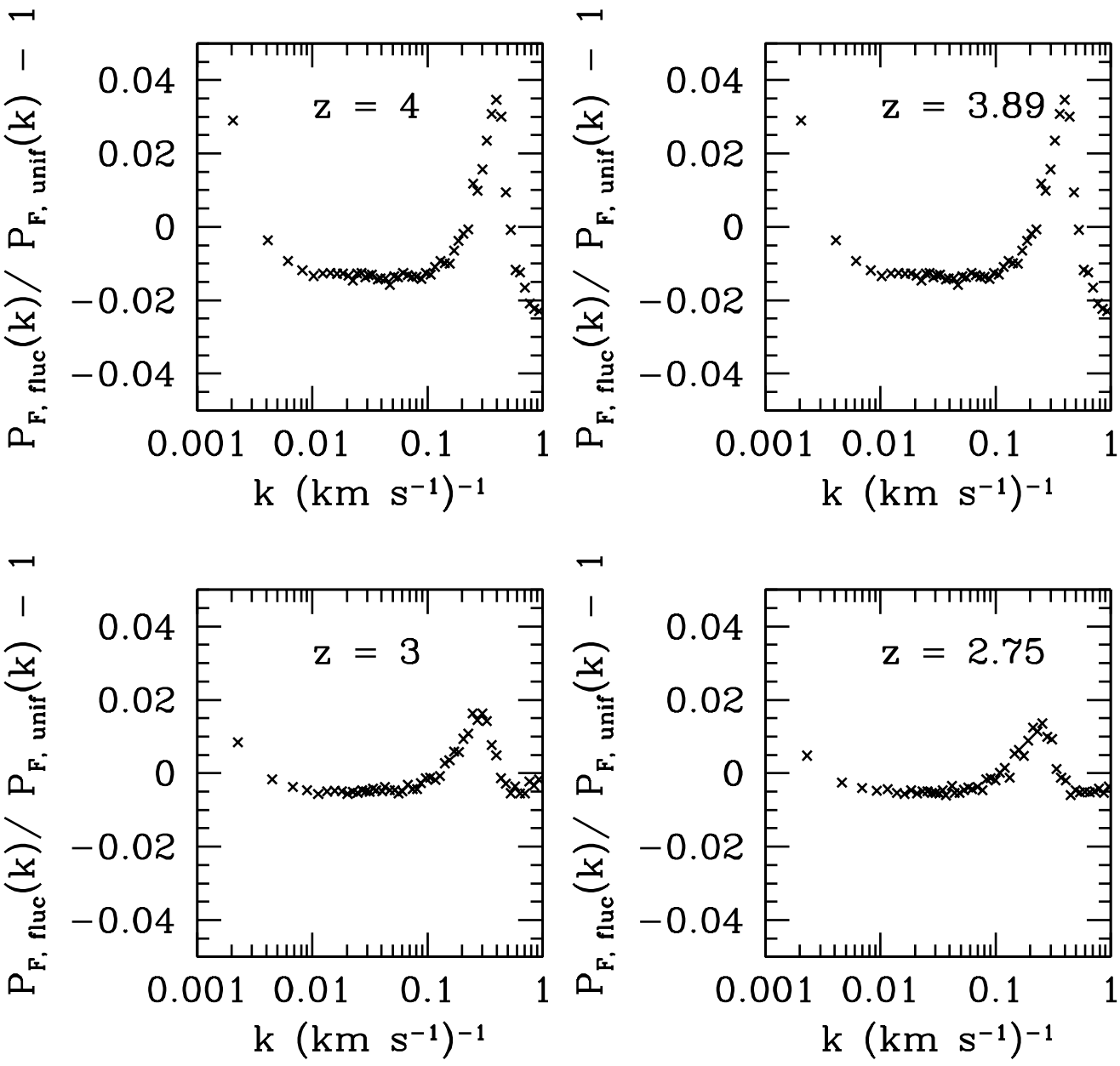

Figure 10. The ratio of the flux power spectrum $P_F(k)$ with UV background fluctuations to the value without, as a function of restframe velocity wavenumber, for Model 4. The results are shown at $z = 2.75$, 3, 3.89 and 4.

noteworthy, as it suggests a given model is a better fit to the data than would be believed on the basis of lower resolution simulations. The larger χ^2 values found for the $60\,h^{-1}\,$Mpc box for $k < 0.032\,(\mathrm{km\,s^{-1}})^{-1}$ suggest that the simulations have still not quite converged on these scales, at least at a resolution of $\Delta r = 58.6\,\mathrm{h^{-1}\,kpc}$, particularly for $z < 3$.

The results in Fig. 8 also show that the goodness-of-fit is highly sensitive to the smoothing. Adopting Gaussian Jeans smoothing instead of smoothing on the mesh

Model	χ^2	$P(>\chi^2)$
1	55.1	0.007
2	38.7	0.192
3	42.3	0.106
4	40.7	0.139
C	44.9	0.065

Table 4. Statistical comparison betwen the model predictions and measurements for the flux power spectrum, combining data at $z = 2.41$, 2.72, 3.00 and 3.89. No adjustment to the equation of state or mean Lyα flux have been made.

scale results in $\chi^2 = 36.6$ for $k < 0.015\,(\mathrm{km\,s^{-1}})^{-1}$, and $P(>\chi^2) = 1.4\times10^{-5}$, in considerably poorer agreement than the mesh-scale smoothing. The agreement is also much poorer than predicted by Croft et al. , although we have not attempted to adjust the mean flux or equation of state to improve the match. Similarly poorer results are found for linear Jeans smoothing. We also compute the effect of a change in the equation of state for the mesh-scale smoothing case, adopting the values for T_0 and γ predicted by the late He II reionization model of Schaye et al. (2000). The agreement considerably worsens, as shown in Fig. 8, resulting in values comparable to the Jeans smoothing cases.

Without direct comparisons to full hydrodynamical simulations of comparably high resolution, it is unclear how much artificial smoothing should be applied to the PM results, or, indeed, how accurately any smoothing scheme may mimic the true underlying hydrodynamical processes. A certain amount of smoothing will always be present in the spectra resulting from thermal broadening and peculiar velocities in the gas, which the PM simulations are able to account for. Indeed, there is a certain amount of degeneracy between the Jeans-scale broadening and changes in the equation of state. The crucial question is whether the pressure forces missing in the PM simulations result in significantly less smoothing than should be physically present to obtain accurate predictions for $P_F(k)$. We are unable to address that question here, but we have demonstrated that the successful application of PM (or HPM) simulations for discriminating between cosmological models on the basis of the flux power spectrum relies critically on the adopted degree of artificial smoothing.

We compare our models with the data of McDonald et al. and Croft et al. (2002b) in Table 4 combining the results at $z = 2.41$, 2.72, 3.00 and 3.89 for $k < 0.015\,(\mathrm{km\,s^{-1}})^{-1}$. The total number of degrees of freedom is 32. We have conservatively adopted mesh-scale smoothing throughout. Within the context of mesh-scale smoothing, the results we provide are upper bounds to the χ^2 for each model, since we have made no effort to improve the fits by making the several adjustments available. Specifically, we have not: 1. adjusted $\bar\tau_\alpha$ to improve the fits, adopting instead the values given by McDonald et al. , or from Table 3 for $z = 2.7$, 2. adjusted the equation of state parameters T_0 and γ, 3. accounted for the spread in the model predictions of $P_F(k)$, or 4. accounted for mode-mode correlations in the power either for the simulations or the data. We confine the comparison to $k < 0.015\,(\mathrm{km\,s^{-1}})^{-1}$, since for this range the model predictions are more stable to changes in the box size, and the range avoids an anomalous low excursion in the measured $P_F(k)$ at $z = 3$ for $k = 0.0179\,(\mathrm{km\,s^{-1}})^{-1}$ with very small error bar.

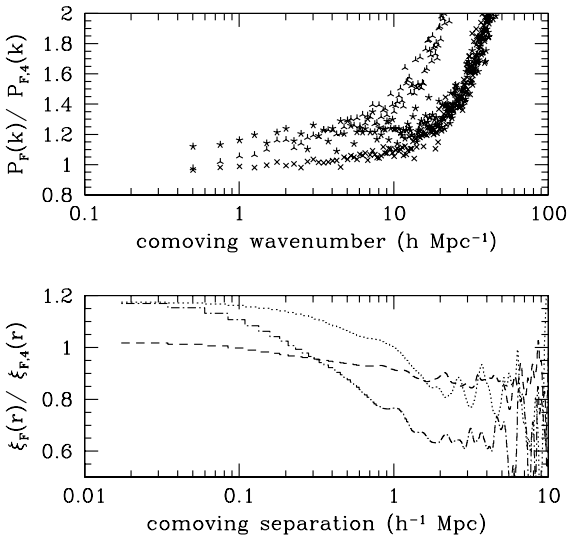

Figure 11. (Upper panel) The ratio of the flux power spectrum for Model 1 (5-pt star), Model 2 (×) and Model 3 (inverted Y) to that of Model 4 at $z = 5$. (Lower panel) The ratio of the flux auto-correlation function for Model 1 (dotted), Model 2 (short dashed) and Model 3 (dot-short dashed) to that of Model 4 at $z = 5$.

The effect of UV background fluctuations on the flux power spectrum is shown in Figs. 9 and 10. Since the UV background fluctuations tend to somewhat suppress the mean flux (boost the mean optical depth) (Paper I), we have re-normalised the uniform background case to the identical mean flux found for the fluctuating background case at each redshift to make a fair comparison. The effect of the fluctuations are most pronounced on large scales and small scales. The small scale peak is on the scale of the absorption line widths and is due in part to a resetting of the mean ionization rate necessary to reproduce the same mean Lyα flux. At intermediate scales the power tends to be somewhat suppressed. The trend at low k of decreasing power with increasing k continues even to $z = 2.75$, although the effect is much reduced and essentially vanishes by $z = 2.41$. The rise at the lowest k value appears to be real, not an artefact of the finite box size, based on convergence tests applied to the concordance model (see Appendix A). At $z = 6$, we also show the small dilution effect of introducing an additional diffuse radiation background of 50% of the average direct contribution from the QSO sources.

The ratios of the flux power spectra for Models 1–3 to Model 4 are shown in Fig. 11 at $z = 5$. The differences between the models are smaller than the effect induced by the UV background fluctuations on the largest scales (smallest wavenumbers). The effect of the fluctuations should be dis-

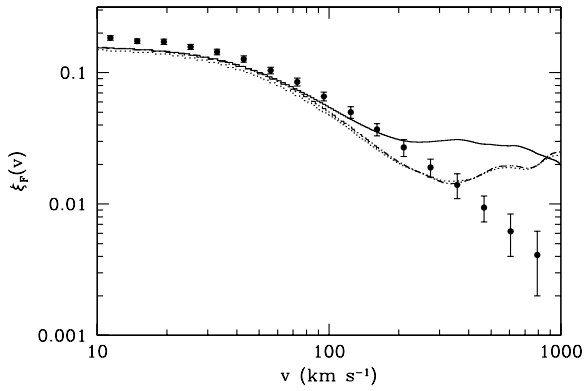

Figure 12. The flux auto-correlation function $\xi_F(v)$ at $z = 2.7$, as a function of restframe velocity separation, for Model 4 (solid) and the concordance model (dashed), assuming Gaussian smoothing on the mesh scale. Also shown is the concordance model using linear Jeans smoothing (dotted). The models are compared with the measurements from Croft et al. (2002b).

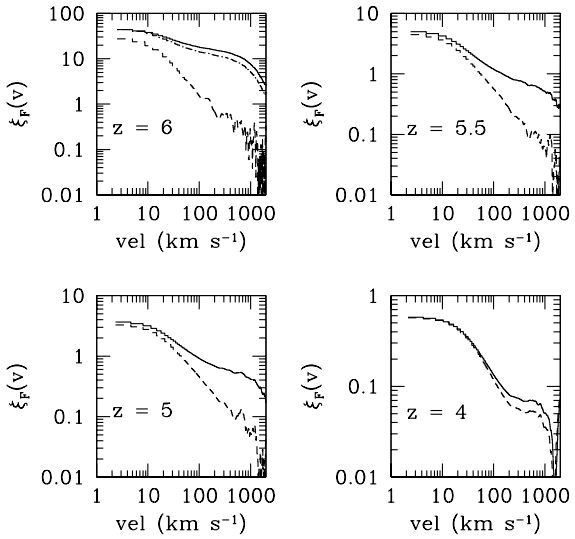

Figure 13. The flux auto-correlation function ξ_F(v), as a function of rest frame velocity separation, for Model 4, with (solid) and without (dashed) UV background fluctuations. Also shown is $\xi_F(v)$ at $z = 6$ including UV background fluctuations, but allowing for a slight suppression due to additional diffuse radiation (dot-dashed line). The results are shown at $z = 4$, 5, 5.5 and 6.

cernable in $z > 5$ spectra of sufficient signal-to-noise ratio within the current precision of the measured cosmological parameters.

4.3 Pixel flux auto-correlation function

We compute the flux auto-correlation function at a velocity separation v for the spectra according to

$$\xi_F(v) = \langle f(v')f(v'-v)\rangle/\langle f\rangle^2 - 1, \quad (9)$$

where $f(v)$ denotes the pixel flux at velocity v, and $\langle f\rangle$ is the measured mean flux at the relevant redshift. The results are shown for Model 4 and the concordance model in Fig. 12 at $z = 2.75$. The data points are from Croft et al. (2002b) at $\langle z\rangle = 2.72$. While the agreement is close at small separations, the model estimates disagree significantly with the measured values. The agreement worsens at large separations, likely due to lack of numerical convergence in the simulation results. We have not attempted to adjust the mean Lyα flux or the equation of state to improve the match.

We compare the flux auto-correlation function with and without UV background fluctuations in Fig. 13. The largest effect is at $z = 6$ and decreases with decreasing redshift. The effect almost disappears by $z = 4$ for velocity separations smaller than $200\,\mathrm{km\,s^{-1}}$. We note that the convergence of the auto-correlation function is not guaranteed for velocity separations exceeding $\sim 100\,\mathrm{km\,s^{-1}}$. At $z = 6$, we also show the small dilution effect of introducing an additional diffuse radiation background of 50% of the average direct contribution from the QSO sources.

The ratios of the flux auto-correlation function for Models 1–3 to Model 4 are shown in Fig. 11 at $z = 5$. The differences between the models are smaller than the effect induced by the UV background fluctuations for small to moderate scales ($< 100\,\mathrm{km\,s^{-1}}$).

5 CONCLUSIONS

We have examined the effect of UV background fluctuations expected from QSO sources on the power spectrum and auto-correlation function of the Lyα forest. To do so, we first performed several sequences of tests to assess the simulation parameters required to reach convergence. We investigate the convergence for different amounts of smoothing meant to mimic hydrodynamical effects, almost all for a fixed equation of state. We note that varying the equation of state will affect the predicted flux power spectrum, and should be included when attempting to constrain cosmological models by comparison with the data. We have not performed an exhaustive search in smoothing algorithms and equations of state to achieve a best match to the data. Our emphasis in this paper is instead to explore the impact these have on the *relative* effect UV background fluctuations are expected to have on the predicted flux power spectrum and auto-correlation function. Our conclusions concerning these tests are (where all length scales are comoving and velocity scales proper):

1. To reach 10% convergence in the required H I photoionization rate Γ_{-12}, a (comoving) spatial resolution of $60\,h^{-1}\,\mathrm{kpc}$ is required.

2. We were not able to reach convergence in the 1D dark matter power spectrum to better than 50% on any scale. Box sizes exceeding $60\,h^{-1}\,$Mpc and/or a spatial resolution of better than $30\,h^{-1}\,$kpc appear to be required at $z = 5$. The convergence requirements are even more severe at lower redshifts. Fortunately good convergence in the 1D matter power spectrum is not required for good convergence in the predicted flux power spectrum because thermal and Doppler broadening of the gas filters out the contribution of the high spatial frequency modes to the H I optical depth.

3. We show that the predicted flux power spectrum $P_F(k)$ is senstitive to the degree of smoothing. A crucial question is how much (or even whether) any additional smoothing to the gas variables should be applied beyond the inherent smoothing of the spectra due to Doppler and peculiar velocity broadening. For the minimal smoothing on the scale of a mesh cell, the minimum resolution and box size required to achieve 10% convergence on (proper) scales $k < 0.015\,(\mathrm{km\,s^{-1}})^{-1}$ is $30\,h^{-1}\,$kpc in a $25\,h^{-1}\,$Mpc box. We were not able to achieve convergence to 10% at larger wavenumbers. Allowing for additional smoothing improves the convergence. With the application of Gaussian Jeans smoothing, it is possible to achieve convergence on all scales $k < 0.1\,(\mathrm{km\,s^{-1}})^{-1}$ to 10% at $z = 5$ for a spatial resolution of at least $60\,h^{-1}\,$kpc in a $30\,h^{-1}\,$Mpc box. With the application of linear Jeans smoothing, we are able to achieve this level of accuracy only for $k \lesssim 0.01\,(\mathrm{km\,s^{-1}})^{-1}$. The convergence requirements become more severe at lower redshifts.

4. We find that introducing Jeans Gaussian or Jeans linear smoothing significantly flattens the predicted flux power spectrum near its peak. Without full hydrodynamical simulations at comparable resolution to our highest resolution simulations in a box size of at least $25\,h^{-1}\,$Mpc, it is not possible to assess whether or not the additional Jeans smoothing, while it improves the convergence properties, also improves the accuracy of the flux power spectrum as predicted from pure gravity simulations.

5. We were unable to obtain convergence in the flux auto-correlation function $\xi_F(k)$ to better than 10% on spatial separations exceeding $\sim 3\%$ of the box size. Comparisons with the data for this statistic appear problematic.

6. A criterion of the level of simulation convergence needed to make a meaningful comparison with observations is the convergence in χ^2 between the simulation predictions and the measured values. We find that χ^2 for the comparison between the predicted and measured $P_F(k)$ continues to decrease with increasing resolution. For our minimal mesh-scale smoothing case, we find differences in the reduced χ^2 at $z \approx 3-4$ of $\sim 50\%$ on going from a resolution of $\sim 60\,h^{-1}\,$kpc to $\sim 30\,h^{-1}\,$kpc in a $30\,h^{-1}\,$Mpc box, and differences of $\sim 20\%$ on increasing the box size to $60\,h^{-1}\,$Mpc at a fixed spatial resolution of $\sim 60\,h^{-1}\,$kpc. Allowing for Jeans smoothing does not greatly improve the convergence in the reduced χ^2 confined to wavenumbers $k < 0.015\,(\mathrm{km\,s^{-1}})^{-1}$. In particular, we find that while the concordance model would be very strongly rejected on the basis of moderate resolution simulations using the minimal amount of mesh-scale smoothing, the model is rejected at only the $\lesssim 2\sigma$ level in our highest resolution simulations. By contrast, when Jeans smoothing is applied, the model is very strongly rejected at all resolutions. We have not explored variations in the equation of state that could potentially improve (or degrade) the agreement.

7. We find significant degeneracy between the smoothing and the equation of state of the baryons. It is unclear how the degeneracy may be removed without performing full hydrodynamic simulations to infer the equation of state of the IGM by comparing with the measured small scale fluctuations of the Lyα forest on the scale of the absorption features. A possibility is to use the measured Doppler parameters to constrain the equation of state (Schaye et al. 2000), but without high resolution simulations in box sizes of at least $\sim 25\,h^{-1}\,$Mpc, it is unclear whether or not the parameters deduced in this way are the optimal ones to use for predicting the flux power spectrum. One complication is the evident need for additional broadening at $z < 3.5$ beyond simple photoionization heating (Theuns et al. 1999; Bryan & Machacek 2000; Meiksin, Bryan & Machacek 2001). The discrepancy in the predicted and measured line widths suggests the underlying physics is still not fully understood, particularly for the moderate to low optical depth lines (Meiksin, Bryan & Machacek 2001).

The simulations are normalised on the basis of the average Lyα flux transmitted through the IGM. We find that there is significantly more accord in the measurements of this parameter than previously recognized once existing constraints are interpreted on a consistent statistical basis.

We assess the possibility of using measurements of the flux power spectrum for inferring the contribution of QSO sources to the metagalactic UV ionizing background. Because of the sparsity of QSOs relative to alternative sources, like galaxies, the UV background contribution from QSOs will exhibit large, spatially correlated fluctuations. We model the fluctuations using Monte Carlo realisations of randomly distributed QSO sources based on QSO counts from the 2dF and SDSS QSO surveys. We estimate the attenuation lengths through the IGM self-consistently from our simulations, requiring a background ionization rate that recovers the measured mean Lyα flux. Because the simulations are not able to recover the measured number of Lyman Limit Systems for $z < 4$, we add their contribution to the attenuation by hand.

The resulting fluctuations increase the required photoionization rates by 5-10% over the uniform background case for $z \leq 5.5$ in order to match the measured mean Lyα fluxes. This is a somewhat smaller effect than was found in Paper I, where only the UV background fluctuations were accounted for and not their spatial correlations. By $z = 6$, we find the trend reverses in the presence of the now very strong UV background correlations: the required photoionization rate is reduced by 10-20% compared with the uniform background case. By contrast, we find that the effect on the cumulative flux distribution increases when the correlations in the UV background fluctuations are included. Previously we found the fluctuations distorted the flux distributions by $\sim 0.2\%$ for $z \geq 5$. Allowing for the correlations increases the effect to 1–1.5%, rendering them somewhat easier to detect.

We find that the magnitudes of the *relative* effects on the 2-pt flux statistics by fluctuations in the UV background are much better converged than the absolute predictions. The ratios of the predicted flux power spectra with and without UV background fluctuations are converged to better than 1% on scales $k < 0.2\,(\mathrm{km\,s^{-1}})^{-1}$ in our simulations, and are

in agreement for Gaussian mesh, Jeans Gaussian and Jeans linear smoothings at this level over these scales. The ratio of the predicted auto-correlation function with and without UV background fluctuations, however, is converged to better than 10% only for velocity separations $\lesssim 200\,\mathrm{km\,s^{-1}}$.

We also find that the UV background fluctuations boost the flux power spectrum at large scales ($k < 0.01\,(\mathrm{km\,s^{-1}})^{-1}$) and small scales ($k \sim 0.2-0.4\,(\mathrm{km\,s^{-1}})^{-1}$, corresponding to the widths of individual absorption features), and suppress the power at intermediate scales. For $z \leq 4$, the effects are small, at the few percent level. At higher redshifts, however, the large scale effect grows due to the increasing strength of the UV background correlations, resulting in a boost in power of over 50% by $z > 5$. By $z = 6$, the background fluctuations produce an upturn in $kP_F(k)/\pi$ towards low k, providing distinctive evidence for the presence of UV background fluctuations, as such an upturn would be unphysical from large-scale structure effects alone. Measuring such an effect at the current level of flux detection is problematic because of the very high Lyα optical depths at these redshifts, but it may become feasible with future Extremely Large Telescope technology, or possibly by searching for the signal at higher orders in the Lyman series where the optical depths are reduced.

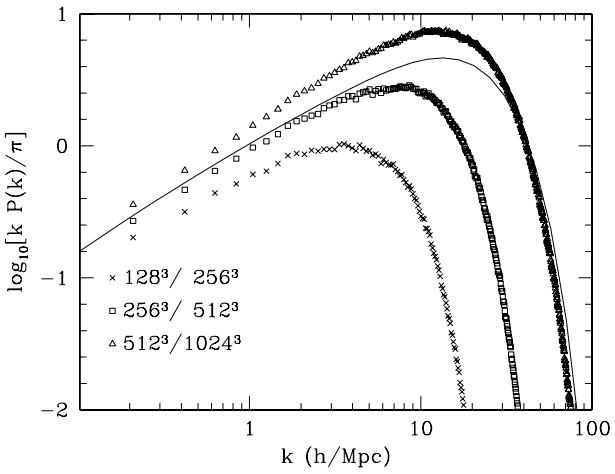

Figure A1. The (real space) 1D matter power spectrum in the concordance cosmology at $z = 5$ from our resolution sequence with 128^3, 256^3 and 512^3 particles and force meshes of 256^3, 512^3 and 1024^3. The solid line shows the predicted 1D spectrum, using the Peacock & Dodds (1996) fitting formulae for the 3D matter power spectrum, Eq. A1, and a Gaussian filtering of 3 mesh cells (FWHM).

ACKNOWLEDGMENTS

M. White was supported by the NSF and NASA. Parts of this work were done on the IBM-SP at the National Energy Research Scientific Computing Center.

APPENDIX A: CONVERGENCE TESTS

Even including only gravitational physics, simulations of the Lyα forest are restricted by two size constraints. High spatial resolution is required to resolve the structure of the absorbers, while a large box size is required both to capture the large-scale power which will affect the velocity widths of the absorption lines as well as to obtain a fair sample of the universe. Although a small box may be adequate to resolve the line structure, if the box is too small the fluctuations corresponding to the scale of the box will become nonlinear, in which case the results are no longer representative of the cosmological model simulated. These numerical effects have been investigated in different contexts by a number of authors (see references in McDonald 2003 for example).

To investigate these effects of numerical resolution further we chose a relatively large box, $30\,h^{-1}$Mpc (comoving) on a side, and simulated the concordance cosmology using 128^3, 256^3 or 512^3 particles (corresponding to 256^3, 512^3 and 1024^3 mesh cells). At the high redshifts of interest to us the fundamental mode of the box is safely in the linear regime, suggesting that the simulation represents a fair sample of the universe. To isolate the effects of numerical resolution from sample variance, we sampled the initial conditions starting at low-k and moving 'outwards' to higher k so that the initial phases and amplitudes of the common modes were identical from simulation to simulation.

The 3D matter power spectrum (not shown) exhibits

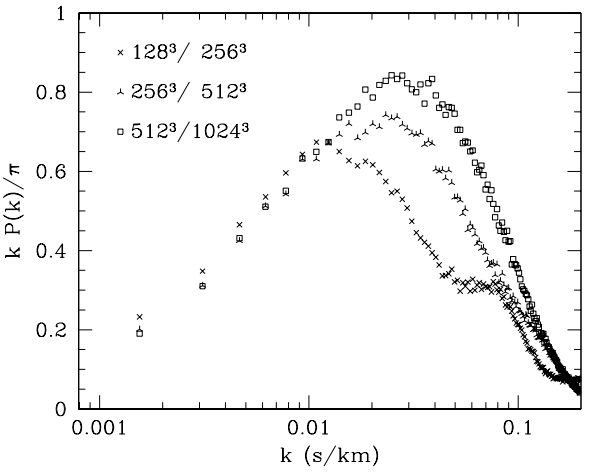

Figure A2. The 1D flux power spectrum in the concordance cosmology at $z = 5$ from our resolution sequence with 128^3, 256^3 and 512^3 particles and force meshes of 256^3, 512^3 and 1024^3. The box size in each run is $30\,h^{-1}$Mpc. These results indicate that our highest resolution runs are converged at better than the 10% level (in power) on scales $k < 0.015\,(\mathrm{km\,s^{-1}})^{-1}$.

the expected behaviour, with the higher resolution simulations having progressively more small-scale power. At $z = 5$ the fundamental mode is safely in the linear regime, with $\Delta^2(k_{\rm fund}) \simeq 0.04$, and the mesh scale is non-linear with $\Delta^2(k_{\rm mesh}) > 10$. The fitting formula of Peacock & Dodds (1996) underestimates the non-linear power by $\mathcal{O}(50)$ per cent. Fig. A1 shows the 1D matter power spectrum, in real space. This is an integral of the 3D spectrum over wavenumbers greater than the 1D wavenumber under consideration:

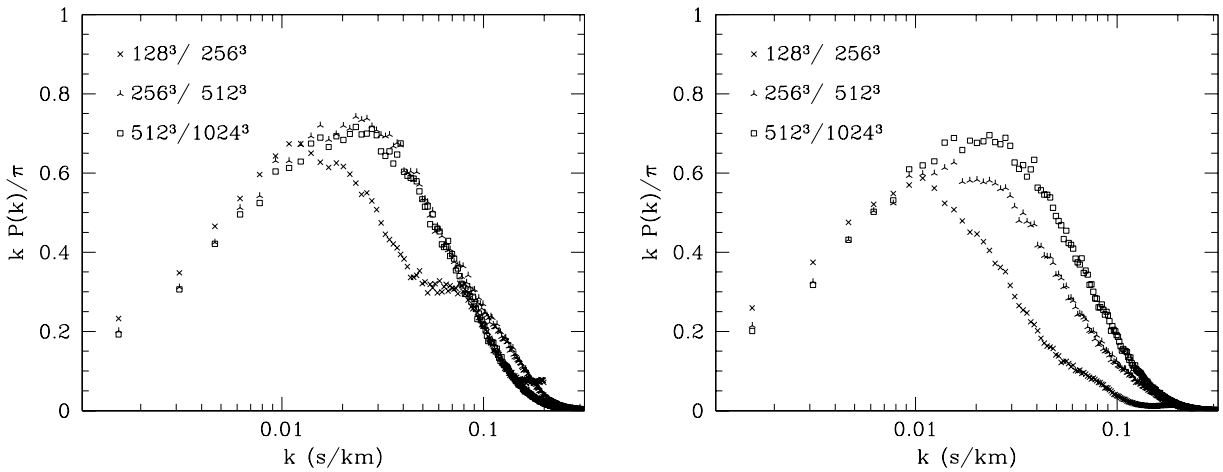

Figure A3. The 1D flux power spectrum in the concordance cosmology at $z = 5$ from a resolution sequence with 128^3, 256^3 and 512^3 particles and force meshes of 256^3, 512^3 and 1024^3. The box size in each run is $30\,h^{-1}$Mpc. (Left) The density and velocity fields are Gaussian smoothed by the Jeans scale. (Right) The density and velocity fields are smoothed by $(1 + [k/k_J]^2)^{-1}$.

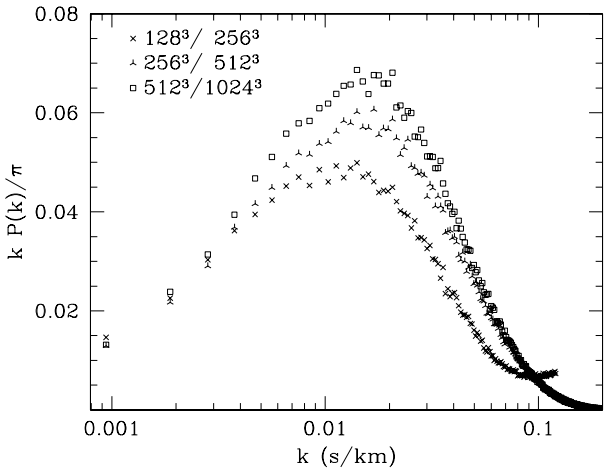

Figure A4. The 1D flux power spectrum in the concordance cosmology at $z = 3$ from a resolution sequence with 128^3, 256^3 and 512^3 particles and force meshes of 256^3, 512^3 and 1024^3. The box size in each run is $60\,h^{-1}$Mpc.

$$\frac{kP(k)}{\pi} = k\int_k^\infty \frac{dy}{y^2}\,\Delta^2_{3D}(y) \qquad . \tag{A1}$$

We find that the numerical results are relatively well fit by the Peacock & Dodds (1996) formalism, if we filter the 3D power spectrum, $\Delta^2_{3D}(k)$, with a Gaussian filter of FWHM 3.2 mesh cells (plotted as the solid line for the highest resolution run) to approximate the finite force resolution of the PM code. Note that missing high-k power in the lower resolution simulations biases the 1D power spectrum low over the whole k-range plotted since much of the long-wavelength power comes from aliasing of 3D short wavelength power. We show in Fig. A2 the power spectra of the flux produced by these 3 runs using a Gaussian smoothing of one mesh cell to define the density and velocity fields. (The flux normalisation is slightly different than used in the text.) From these results we infer that, for the relatively high redshifts of interest, a $30\,h^{-1}$Mpc box with 512^3 particles and a 1024^3 force mesh produces spectra converged to better than the 10 per cent level.

Similar conclusions were found by McDonald (2003), though our convergence is not quite at the level quoted therein. Part of the reason for this is the treatment of small-scale power in the simulations. To investigate this we modified our smoothing procedure following Gnedin & Hui (1998) to mimic the effects of thermal pressure on the baryonic component, using either Gaussian or linear smoothing as described in Section 2 above.

We show in Fig. A3 that the Gaussian smoothing method, used by Zaldarriaga et al. (2001), improves the convergence. This is to be expected since the Jeans scale here is close to the mesh size of our intermediate resolution run. We found that pure linear theory smoothing introduced numerical artifacts unless it was supplemented with our standard single mesh cell Gaussian smoothing, so we show in Fig. A3 the results of this hybrid. For the smaller runs the Gaussian smoothing dominates, but at higher resolution the linear Jeans smoothing is suppressing small-scale power as well.

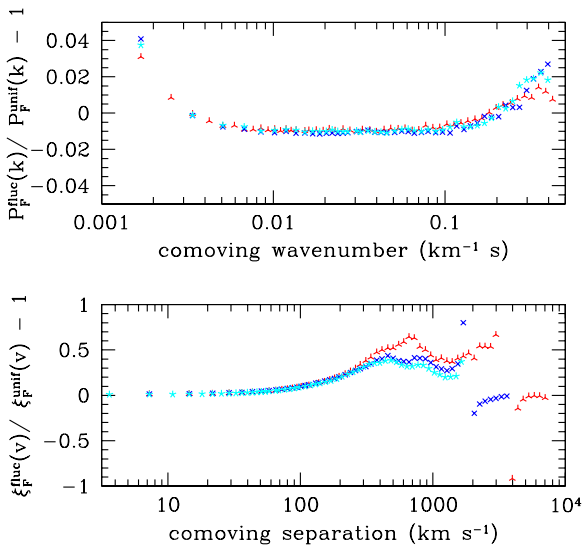

Figure A5. The ratios of the (upper panel) 1D flux power spectrum and (lower panel) flux auto-correlation function, with and without UV background fluctuations, in the concordance cosmology at $z = 4$ from a resolution sequence with comoving grid size $\Delta r = 58.6\,h^{-1}$ kpc , in boxes of comoving sides $30\,h^{-1}$ Mpc (×) and $60\,h^{-1}$ Mpc (inverted Y), and with a comoving grid size $\Delta r = 29.3\,h^{-1}$ kpc in a box of comoving side $30\,h^{-1}$ Mpc (5-pt star).

The convergence becomes fractionally better if we increase T_0 or decrease γ. It becomes only slightly worse if we lower T_0 to 10^4K. A further sequence reducing the box size (not shown here) suggests that we can safely reduce the volume simulated to a box of side $25\,h^{-1}$Mpc if we are interested in the Lyα forest at high redshift. This makes the mesh scale slightly smaller, capturing the features in the forest slightly better, thus we have used $25\,h^{-1}$Mpc thoughout.

Finally, we show in Fig. A4 a convergence study at lower redshift ($z = 3$) in a larger box ($60\,h^{-1}$Mpc). The power spectrum in the larger box follows closely that of the smaller box at half the resolution. It thus departs significantly from that in the $30\,h^{-1}$Mpc box at $k \simeq 0.01$ km^{-1} s for the highest resolution runs, slightly earlier than might be expected from Fig. A2 due to the increased non-linear scale.

In Fig. A5, we show a convergence sequence at $z = 4$ for models including fluctuations in the UV background. The UV background fluctuations are based on the QSO counts with $\beta_1 = 3.2$ described in the text, with an added diffuse component increasing the ionization rate by 40% to reproduce the measured average flux. The rise in $P_F(k)$ at the lowest k-values appears to be real. The effect of the UV background fluctuations on the flux auto-correlation becomes poorly determined for velocity separations exceeding 300 km s^{-1} .

We show in Fig. A6 that the Gaussian and linear Jeans smoothing improve the convergence of the flux auto-correlation function over the Gaussian single-mesh scale smoothing. For 256^3 particles on a 512^3 force mesh, the

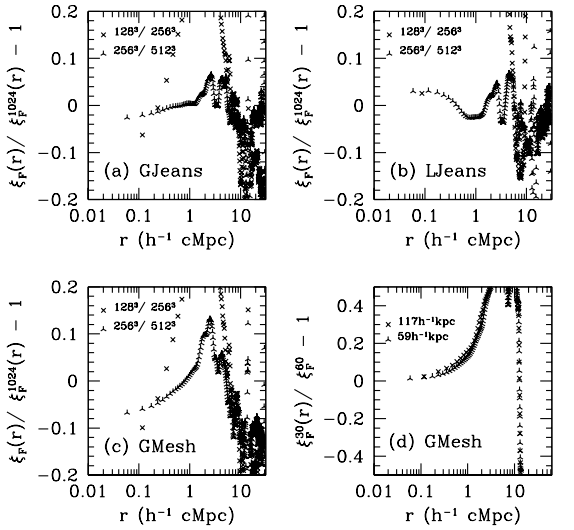

Figure A6. The error in the 1D flux auto-correlation function in the concordance cosmology at $z = 4$ from (panels a–c) a resolution sequence in a box of comoving size $30\,h^{-1}$Mpc with 128^3 and 256^3 particles and force meshes of 256^3 and 512^3, compared with 512^3 particles and a force mesh of 1024^3, and from (panel d) a box size sequence comparing boxes of comoving size $30\,h^{-1}$Mpc with $60\,h^{-1}$Mpc for (comoving) force mesh resolutions of $\Delta r = 117\,\mathrm{h^{-1}\,Mpc}$ and $58.6\,\mathrm{h^{-1}\,Mpc}$.

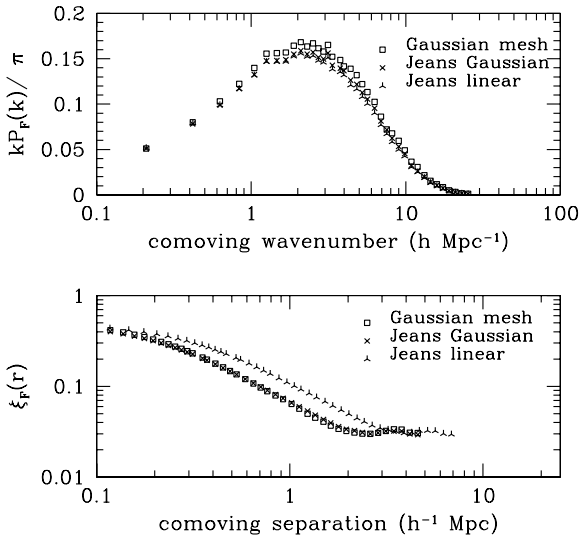

Figure A7. The 1D flux power spectrum (upper panel) and flux auto-correlation function (lower panel) in the concordance cosmology at $z = 4$ for Gaussian smoothing on the mesh size, Jeans Gaussian smoothing and Jeans linear smoothing. The box size in each run is $30\,h^{-1}$Mpc.

Jeans smoothings give convergence to better than 5% on comoving separations of $r < 3\,h^{-1}$Mpc, or 10% of the box size. The single-mesh Gaussian smoothing converges to only 15% on these scales. Also shown is a comparison of the single-mess Gaussian smoothing for comoving box sizes of $30\,h^{-1}$Mpc and $60\,h^{-1}$Mpc, at two spatial resolutions, showing convergence to 10% only for comoving separations of $r < 1\,h^{-1}$Mpc, or 3% of the box size.

While the smoothing schemes introduced above improve convergence, this does not guarantee that they coverge to the correct power spectra, as would be computed using a full hydrodynamical scheme. A direct comparison is still prohibitively computationally expensive because of the wide range in lengthscales required both to resolve the non-linear structures into which the bulk of the IGM collapses and to capture sufficient large-scale power to obtain an accurate computation of the flux power spectrum and flux auto-correlation function. The most we can demonstrate is that the results are not excessively sensitive to the smoothing scheme.

In Fig. A7, we compare the three smoothing methods for the concordance model at $z = 4$. The power spectra for both Jeans smoothings agree to within 1–2%, although they are suppressed in power compared with the Gaussian single-mesh smoothing by as much as 8% near the peak. By contrast, both Gaussian smoothings result in flux auto-correlation functions agreeing to 3%, while the linear Jeans smoothing results in an excess of correlations of as much as 60%. These results leave ambiguous which smoothing method may be most accurate. For simplicity, we retain the mesh-scale Gaussian smoothing for the main results in the text, but make reference to alternative smoothings.

The different smoothing methods result in different rates of convergence of the metagalactic ionization rate Γ_{-12} required to match the measured mean Lyα flux, as shown in Fig. A8. For a force mesh of 1024^3, the different methods yield ionization rates agreeing to 2%. This is comparable to the difference between meshes of sizes 512^3 and 1024^3 for each smoothing, except for the linear Jeans smoothing, for which the difference is 4%.

APPENDIX B: MEAN FLUX

The simulations leave unspecified the ionization level of the IGM. As a consequence, the flux normalisation of the spectra is undetermined. We fix the normalisation of the simulations by adjusting A in eq. 3 to match the measured mean Lyα flux values as given by Fan et al. (2002) in their Figure 1 for $z \geq 4$, as tabulated in Table 3. For $z < 3.89$, we estimate the mean flux from a set of published Keck HIRES spectra, as described below.

The measurements of the mean flux have proven difficult, largely due to uncertainties in the QSO continuum across the absorbing region. Deriving error bars on the estimates is even more difficult because of difficulties in measuring the error on the continuum estimate, and because of flux correlations between pixels. PRS used bootstrap resampling to estimate the errors on their fit to the mean Lyα optical depth $\bar{\tau}_\alpha$, obtaining $\bar{\tau}_\alpha = A(1+z)^{1+\gamma}$, with $\gamma = 2.46 \pm 0.37$ and $A = 0.0175 - 0.0056\gamma \pm 0.0002$. The interpretation of the

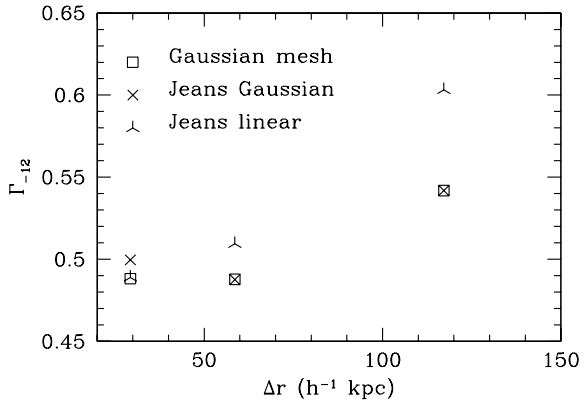

Figure A8. The convergence of the required metagalactic ionization rate Γ_{-12}, in units of $10^{-12}\,\mathrm{s}^{-1}$, at $z = 4$ for force mesh (comoving) resolutions of $\Delta r = 29.3\,\mathrm{h}^{-1}\,\mathrm{kpc}$, $58.6\,\mathrm{h}^{-1}\,\mathrm{kpc}$ and $117\,\mathrm{h}^{-1}\,\mathrm{kpc}$, for Gaussian smoothing on the mesh size, Jeans Gaussian smoothing and Jeans linear smoothing. Results shown are for the concordance model. The comoving box size in each run is $30\,h^{-1}$Mpc.

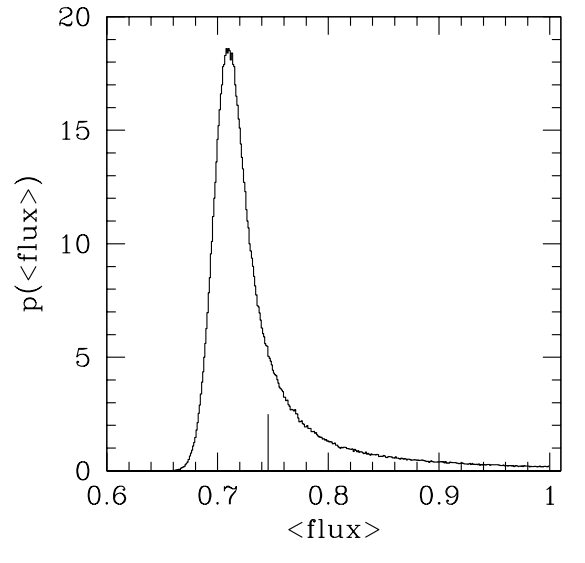

Figure B1. The probability distribution of the mean absorbed Lyα flux at $z = 2.72$ according to the estimate of PRS. The long vertical tick mark indicates the average mean flux.

z	PRS	SS87	KCD	this paper
4.0	$0.46^{+0.06}_{-0.08}$	0.48 ± 0.05	0.49 ± 0.01	0.47 ± 0.03
3.89	$0.48^{+0.05}_{-0.08}$	0.51 ± 0.05	0.51 ± 0.01	0.48 ± 0.02
3.0	$0.69^{+0.04}_{-0.05}$	0.71 ± 0.03	0.71 ± 0.01	0.70 ± 0.02
2.75	$0.74^{+0.04}_{-0.05}$	0.76 ± 0.03	0.76 ± 0.01	0.74 ± 0.04
2.41	$0.80^{+0.03}_{-0.04}$	0.82 ± 0.02	0.82 ± 0.01	——-

Table B1. Estimates for $\langle\exp(-\tau)\rangle$ using fits to $\bar{\tau}_\alpha$ from Press, Rybicki & Schneider (1993) (PRS), Zhang et al. (1997) as fit to the D_A values of Steidel & Sargent (1987) (SS87), and Kim, Cristiani & D'Odorico (2001) (KCD). Also shown are the values adopted in this paper.

error is not completely clear. Seljak, McDonald & Makarov (2003) argue that, if the errors from PRS are interpreted as Gaussian, then the PRS fit results in both a bias and large error estimate for $\bar{\tau}_\alpha$. Seljak et al. find at $z = 2.72$, $\langle\bar{\tau}_\alpha\rangle = 0.29 \pm 0.14$, where $\langle\ldots\rangle$ denotes an average over Gaussian distributions for A and γ, while using the mean values of A and γ would instead give $\bar{\tau}_\alpha = 0.35$. The error they quote, however, is the statistical *rms* on $\bar{\tau}_\alpha$, which carries little probabilistic meaning since the resulting probability distribution of $\bar{\tau}_\alpha$ is highly skewed. Moreover, they allowed for unphysical values of $\bar{\tau}_\alpha < 0$ in their averaging. Truncating the distribution to $\bar{\tau}_\alpha \geq 0$ yields an *rms* of 0.09 instead, which we estimate from a Monte Carlo calculation. In terms of an equivalent Gaussian 1σ error spread, defined so that the probabilities of obtaining a value 1σ above or 1σ below the mean are each 0.16, the equivalent 1σ error spread in $\bar{\tau}_\alpha$ is $\langle\bar{\tau}_\alpha\rangle = 0.30^{+0.06}_{-0.05}$, truncating to $\bar{\tau}_\alpha \geq 0$.

Relating the mean optical depth to the mean absorbed flux and its error is not straightfoward. Instead it is better to start with the distributions for A and γ and estimate $\langle\exp(-\bar{\tau}_\alpha)\rangle$ directly. The resulting probability distribution for the mean flux at $z = 2.72$ is shown in Figure B1. The peak of the distribution is at $\exp(-\bar{\tau}_\alpha) = 0.71^{+0.03}_{-0.02}$, where the error bars refer to the range in the mean flux enclosing 68% of the probability. The mean is $\langle\exp(-\bar{\tau}_\alpha)\rangle = 0.75 \pm 0.07$, where the error is the *rms*, and the distribution was truncated to $\bar{\tau}_\alpha \geq 0$. Adopting the 1σ equivalent probabilistic interpretation of the error, as above, gives instead a mean of $\langle\exp(-\bar{\tau}_\alpha)\rangle = 0.75^{+0.04}_{-0.05}$. Because of the skewed nature of the probability distribution, the estimate of the error for any quantity depending on the mean flux must take into account the full probability distribution of the mean flux.

For $z < 4$, we use the published Keck HIRES spectra used by Meiksin, Bryan & Machacek (2001) for testing models of the Lyα forest. These spectra cover the redshift range $2.5 < z < 3.7$. We estimate the mean flux from each spectrum over a narrow redshift interval ($\Delta z = 0.1-0.3$) centred at each redshift considered, and average the results, adopting the error in the mean as our error estimate. We also allow for small systematic offsets in the continuum level (typically 1–4%), as provided by Meiksin et al. for the two best-fitting models to the flux distribution (which are ΛCDM models similar to those considered in this paper). We estimate the error in the systematic offset from the spread between the best-fitting models (1–2% of the continuum level), and add this linearly to the error in the mean. (Since the error is sys-

tematic rather than statistical, adding the error in quadrature would be inappropriate.)

For $z = 3.89$, we adopt the value of McDonald et al. (2000) of 0.48 ± 0.02. For $z = 4.0$, we use the best-fit of Songaila & Cowie (2002) to the measured redshift trend (their eq.[19]), to obtain a value for the mean flux of 0.47. We also linearly extrapolate the values of Songaila & Cowie (2002) at $\langle z \rangle = 4.34$ and 4.07 down to $z = 4.0$, obtaining a mean flux of 0.36 ± 0.03. The difference appears due to a single outlying measurement which substantially lowers the mean. We shall consider both values, noting that the larger one better matches the trend in Table B1.

For comparison, we also show the estimates, using the above procedure as applied to the fit to $\bar{\tau}_\alpha$ of Press et al. , based on similar estimates from Kim, Cristiani & D'Odorico (2001) with $A = 0.0144 - 0.00471\gamma$ and $\gamma = 2.43 \pm 0.17$ (which we infer from their error estimates for A and γ), and the fit by Zhang, Anninos, Norman & Meiksin (1997) to the flux decrement values (D_A) of Steidel & Sargent (1987), $A = 0.0028 \pm 0.0004$, $\gamma = 2.46$ (fixed). The errors provided correspond to the equivalent 1σ Gaussian errors, as described above.

The results are tabulated in Table B1. All the estimates are found to be in accord, including those of Press et al. This is noteworthy in that the estimates that had been made using the best value for $\bar{\tau}_\alpha$ from Press et al. generally gave values significantly higher than measured using high resolution spectra. Estimating the mean flux including the errors as we have done shows that these results are actually in agreement with the estimates from the higher resolution data. It is also noteworthy that the estimates based on the moderate resolution data of Steidel & Sargent are nearly identical to those using the $\bar{\tau}_\alpha$ fit of Kim et al. , which is based on a compilation of several high resolution spectra. The agreement in the determinations of the mean flux between the moderate and high resolution spectra suggests that moderate resolution spectra, like those of the Sloan Digital Sky Survey, should, in principle, be adequate for measuring the mean flux. At attempt to measure the mean flux from the Sloan QSO survey was made by Bernardi et al. (2003). The values found at $z = 2.41$, 2.75, 3.0 and 3.89 are, respectively (as given in their Fig. 21), $\langle \exp(-\tau) \rangle = 0.74 \pm 0.03$, 0.71 ± 0.01, 0.65 ± 0.01, and 0.36 ± 0.02. These all lie systematically low compared with the values listed in Table B1. The reasons for the discrepancy are unclear.

Since the mean flux is the quantity of interest for normalising the Lyα forest simulations, we use direct measurements of the mean flux to normalise our simulations rather than estimates of the mean Lyα optical depth. Historically, $\bar{\tau}_\alpha$ was of interest in the context of models for which the absorption was produced by discrete aborption clouds rather than modulations in a continuous medium. For the purposes of studies of the IGM under the current continuum model of its structure, $\bar{\tau}_\alpha$ has lost most of its significance; the mean flux is almost always to be preferred. An exception is in estimating the contribution of known discrete systems to the mean flux. Of particular interest is the contribution from Damped Lyα Absorbers (DLAs). The contribution of discrete absorption systems to $\bar{\tau}_\alpha$ is given by (eg, Meiksin & Madau 1993; PRS)

$$\bar{\tau}_{\rm eff} = \frac{1+z}{\lambda_\alpha} \int dN_{\rm HI} \frac{\partial^2 N}{\partial N_{\rm HI} \partial z} w(N_{\rm HI}), \qquad \text{(B1)}$$

where $w(N_{\rm HI})$ is the equivalent width corresponding to a system with H I column density $N_{\rm HI}$, and λ_α is the (rest) wavelength of the Lyα transition. Here, $\partial^2 N/(\partial N_{\rm HI} \partial z)$ is the H I column density distribution at redshift z, assumed to vary slowly over the width of an absorption feature. The $N_{\rm HI}$ distribution is estimated to be a power law $\propto N_{\rm HI}^{-\beta}$ with $\beta = 1.5$, with a possible high $N_{\rm HI}$ cut-off (Storrie-Lombardi, Irwin & McMahon 1996). Since DLAs are on the square-root part of the curve of growth ($w \propto N_{\rm HI}^{1/2}$), $\bar{\tau}_{\rm DLA}$ is logarithmically divergent at the upper end. Even if the distribution steepens at the upper end, as suggested by Storrie-Lombardi et al. , the statistics are so poor that the contribution of DLAs to $\bar{\tau}_\alpha$ is highly uncertain. Seljak et al. claim to have adjusted their error estimate of $\bar{\tau}_\alpha$ to allow for DLAs, although they give no details of their procedure. In view of the uncertainty in $\bar{\tau}_{\rm DLA}$, the most reliable approach is to use only spectral regions that are clean of DLA contamination to estimate the mean flux.

REFERENCES

Bernardi M., et al. , 2003, AJ, 125, 32
Bond J. R., Wadsley J. W., 1997, in Petitjean P., Charlot S., eds, Structure and Evolution of the Intergalactic Medium from QSO Absorption Line Systems. Editions Frontières, Paris, p. 143
Boyle B. J., Shanks T., Peterson B. A., 1988, MNRAS, 235, 935
Boyle B. J., Shanks T., Croom S. M., Smith R. J., Miler L., Loaring N., Heymans C., 2000, MNRAS, 317, 1014
Cen R., Miralda-Escudé J., Ostriker J. P., Rauch M., 1994, ApJ, 437, L9
Croft R. A. C., Hernquist L., Springel V., Westover M., White M., 2002a, ApJ, 580, 634
Croft R.A.C., Weinberg D. H., Katz N., Hernquist L., 1998, ApJ, 495, 44
Croft R. A. C., Weinberg D. H., Pettini M., Hernquist L., Katz N., 1999, ApJ, 520, 1
Croft R. A. C., et al. , 2002b, ApJ, 581, 20
Fan X., et al. , 2001, AJ, 121, 54
Fan X., et al. , 2002, AJ, 123, 1247
Fardal M., Shull M., 1993, ApJ, 415, 524
Ferguson H. C., Dickinson M., Papovich C., 2002, ApJ, 569, 65
Gardner J. P., Katz N., Hernquist L., Weinberg D. H., 1997, ApJ, 484, 31
Gnedin N. Y., Hui L., 1998, MNRAS, 296, 44
Gnedin N.,Y., Hamilton A.J.S., 2002, MNRAS, 334, 107
Haardt F., Madau P., 1996, ApJ, 461, 20
Hernquist L., Katz N., Weinberg D., Miralda-Escudé J., 1996, ApJ, 457, L51
Kim T.-S., Cristiani S., D'Odorico S., 2001, A&A, 373, 757
McDonald P., 2003, ApJ, 585, 34
Madau P., Meiksin A., 1994, ApJ, 433, L53
Meiksin A., 1994, ApJ, 431, 109
Meiksin A., 2000, MNRAS, 314, 566
Meiksin A., Bryan G. L., Machacek M. E., 2001, MNRAS, 327, 296
Meiksin A., Madau P., 1993, ApJ, 412, 34
Meiksin A., White M., 2001, MNRAS, 324, 141
Meiksin A., White M., 2003, MNRAS, 342, 1205 (Paper I)
Peacock J.A, Dodds S.A., 1996, MNRAS, 280, 19
Petitjean P., Mücket J. P., Kates R. E., 1995, A&A, 295, L9
Ostriker J., Steinhardt P.J., 1995, Nature, 377, 600

Press W. H., Rybicki G. B., Schneider D. P., 1993, ApJ, 414, 64 (PRS)
Reimers D., Köhler S., Wisotzki L., Groote D., Rodriguez-Pascual P., Wamsteker W., 1997, A&A, 327, 890
Schaye J., Theuns T., Leonard A., Efstathiou G., 1999, MNRAS, 310, 57
Schaye J., Theuns T., Rauch M., Efstathiou G., Sargent W. L. W., 2000, MNRAS, 318, 817
Seljak U., McDonald P., & Makarov A., 2003, MNRAS, in press (astro-ph/0302571)
Songaila A., Cowie L. L., 2002, AJ, 123, 2183
Steidel C. C., Pettini M., Adelberger K. L., 2001, ApJ, 546, 665
Steidel C. C., Sargent W. L. W., 1987, ApJ, 313, 171
Stengler-Larrea E. A. et al. , 1995, ApJ, 444, 64
Storrie-Lombardi L. J., Irwin M. J., McMahon R. G., 1996, MNRAS, 282, 1330
Theuns T., Leonard A., Efstathiou G., 1998, MNRAS, 297, L49
Theuns T., Leonard A., Schaye J., Efstathiou G., 1999, MNRAS, 303, L58
Zaldarriaga M., Hui L., Tegmark M., 2001, ApJ, 557, 519
Zhang Y., Anninos P., Norman M. L., 1995, ApJ, 453, L57
Zhang Y., Anninos P., Norman M. L., Meiksin A., 1997, ApJ, 485, 496
Zhang Y., Meiksin A., Anninos P., Norman M. L., 1998, ApJ, 495, 63
Zheng W., Kriss G. A., Telfer R. C., Grimes J. P., Davidsen A. F., 1997, ApJ, 475, 469
Zuo L., 1992a, MNRAS, 258, 36
Zuo L., 1992b, MNRAS, 258, 45
Zuo L., Bond J. R., 1994, ApJ, 423, 73
Zuo L., Phinney E. S., 1993, ApJ, 418, 28